

A scalable estimator of high-order information in complex dynamical systems

Alberto Liardi,^{1,*} George Blackburne,^{2,1} Hardik Rajpal,³ Fernando E. Rosas,^{3,4} and Pedro A.M. Mediano^{1,2}

¹*Department of Computing, Imperial College London, UK*

²*Department of Experimental Psychology, University College London, UK*

³*Center for Complexity Science, Department of Mathematics, Imperial College London, UK*

⁴*Sussex AI and Sussex Centre for Consciousness Science, University of Sussex, Brighton, UK*

Our understanding of neural systems rests on our ability to characterise how they perform distributed computation and integrate information. Advances in information theory have introduced several quantities to describe complex information structures, where collective patterns of coordination emerge from high-order (i.e. beyond-pairwise) interdependencies. Unfortunately, the use of these approaches to study large neural systems is severely hindered by the poor scalability of existing techniques. Moreover, there are relatively few measures specifically designed for multivariate time series data. Here we introduce a novel measure of information about macroscopic structures, termed \mathcal{M} -information, which quantifies the high-order integration of information in complex dynamical systems. We show that \mathcal{M} -information can be calculated via a convex optimisation problem, and we derive a robust and efficient algorithm that scales gracefully with system size. Our analyses show that \mathcal{M} -information is resilient to noise, indexes critical behaviour in artificial neuronal populations, and reflects task performance in real-world mouse brain activity data. Furthermore, \mathcal{M} -information can be incorporated into existing information decomposition frameworks to reveal a comprehensive taxonomy of information dynamics. Taken together, these results help us unravel collective computation in complex neural systems.

I. INTRODUCTION

How can the collective interactions of a neural system be best measured and understood? Answering this question promises to reveal the functional architecture of both biological and artificial neural networks. Specifically, understanding how these systems integrate information across spatiotemporal scales will prove instrumental in uncovering the mechanisms that support intelligent adaptive behaviour [1–7].

A defining feature of complex neural systems is their ability to exhibit non-linear emergent dynamics, arising from interactions that go beyond simple pairwise relationships. These *high-order behaviours* [8] reflect the system’s capacity to generate collective effects that are not reducible to individual components or their pairwise connections. Importantly, such high-order effects are responsible for the emergence of macroscopic, systemic-level properties that are more functionally informative and causally proximal to cognition and adaptive behaviour [9, 10].

A variety of mathematical frameworks have been developed to characterise high-order phenomena, originating in fields such as network theory [11–13], algebraic topology [14–16], and information theory [17–19]. Within the information-theoretic framework, high-order phenomena have been shown to underpin a wide range of neurobiological functions – including visual processing [11, 20], sensory integration [21, 22], development and ageing [23, 24], and consciousness [10, 25, 26]. Similar effects have been observed in artificial neuronal networks [27–31], suggesting shared organisational principles across both systems in-vivo and in-silico.

Despite the vast proliferation of measures of high-order phenomena (see Sec. V), no approach has been able to provide a comprehensive quantification of the collective structure of a complex system while remaining computationally feasible. Accordingly, the main challenge in developing a measure of high-order information is to devise a measure that: (1) captures all high-order interdependencies between multivariate variables, (2) scales efficiently with the system size, (3) is tailored to dynamical systems composed of parts evolving jointly over time, and (4) identifies the high-order contributions on their own terms, rather than expressing a balance

* a.liardi@imperial.ac.uk

between high- and low-order interactions. Existing approaches meet some of these criteria: for instance, conditions (1) and (2) are resolved by the methods in Refs. [32–34], while (1), (3) and (4) are satisfied by some information decomposition frameworks [35, 36]. However, to the best of our knowledge, no existing measure successfully addresses all four challenges simultaneously.

To tackle this issue, here we introduce a novel estimator of high-order information in complex dynamical systems, which we term \mathcal{M} -information. Our approach builds on the notion of *union information* introduced by Bertschinger *et al.* and Griffith and Koch [37, 38], which we extend to more general scenarios comprising multiple inputs and outputs.

We begin by introducing the mathematical foundations of \mathcal{M} -information and propose a practical implementation for its computation that is robust and easily scalable to large systems. Then, we show that our multivariate formulation of \mathcal{M} -information has a natural application to dynamical systems, validating this property both on synthetic dynamical models and empirical Neuropixel data from mice performing a visual discrimination task.

Our main original contributions include:

1. We introduce the \mathcal{M} -information, a novel multivariate information-theoretic measure of high-order dependencies in complex systems;
2. We show that \mathcal{M} -information can be efficiently calculated in Gaussian distributions via a convex optimisation problem;
3. We illustrate the behaviour of \mathcal{M} -information on synthetic models, and demonstrate its potential for empirical applications using real-world brain activity data;
4. We integrate \mathcal{M} -information with existing information decomposition frameworks, providing a fine taxonomy of information flow in dynamical systems.

II. A MEASURE OF HIGH-ORDER INFORMATION

A. Preliminaries: Quantifying union information

Consider a scenario where d_X random variables $\mathbf{X} = \{X_1, \dots, X_{d_X}\}$, referred to as *sources*, are used to obtain information about another variable Y , referred to as *target*. Let’s denote as $P(X_1, \dots, X_{d_X}, Y)$ the joint distribution of sources and target, and as $P(X_i, Y)$ the pairwise marginal distribution between X_i and Y . The *union information* that a set of sources \mathbf{X} provide about a target Y is defined as

$$I^\cup(\mathbf{X}; Y) := \min_{Q \in \Delta_P} I_Q(\mathbf{X}; Y), \quad (1)$$

where $\Delta_P := \{Q \in \Delta : Q(X_i, Y) = P(X_i, Y) \forall i\}$ contains the probability distributions on (\mathbf{X}, Y) with same marginals as P , Δ is the full set of all probability distributions on (\mathbf{X}, Y) , and I_Q denotes the mutual information calculated on the distribution Q . Analogously to the notion of the union operation in set theory, the union information can be conceived as capturing the “union” of all the pieces of information that each source X_i has about the target Y [37, 38]. Note that the union information only depends on pairwise marginals, and hence serves as a proxy for the system’s low-order information [38].

Both Bertschinger *et al.* [37] and Griffith and Koch [38] introduced I^\cup with the aim of calculating a full decomposition of the mutual information $I(\mathbf{X}; Y)$ (typically called the BROJA-PID [39], but also sometimes referred to as \sim -PID [40]) that is grounded in operational principles from game theory [37] and network information theory [41]. Nonetheless, the union information is an interesting measure of low-order information in its own right [42]. Computationally, calculating the minimum in Eq. (1) for arbitrary distributions is highly non-trivial, with multiple implementations available [39, 43–45]. Conveniently, calculation in Gaussian systems is tractable, and efficient gradient-based methods are available [40].

B. Defining union information in multivariate systems

Let’s now investigate how to formulate a more general version of union information, which can be used to analyse multivariate dynamical systems – such as the activity of multiple neuronal populations evolving

jointly over time. For this, let's consider $\mathbf{X} = \{X_1, \dots, X_{d_X}\}$ source variables and $\mathbf{Y} = \{Y_1, \dots, Y_{d_Y}\}$ target variables jointly following a probability distribution $P \in \Delta$. Our approach is to formally posit a multivariate extension of Eq. (1) that captures the low-order information shared between sources and targets, which we informally call “double union information” and denote as \mathcal{W} (corresponding to two union signs). Following this rationale, the mutual information between sources and targets is decomposable as

$$I(\mathbf{X}; \mathbf{Y}) = \mathcal{W}(\mathbf{X}; \mathbf{Y}) + \mathcal{M}(\mathbf{X}; \mathbf{Y}), \quad (2)$$

where the \mathcal{M} -information is the complement of the \mathcal{W} -information, and as such, it must contain all high-order interactions.

Inspired by Bertschinger *et al.* [37], our next step is to specify desiderata for properties of \mathcal{W} and \mathcal{M} so that their functional form can be determined. We propose the following:

Assumption 1 (*Pairwise dependence*). $\mathcal{W}(\mathbf{X}; \mathbf{Y})$ should only depend on the pairwise marginal distributions $P(X_i, Y_j)$.

Assumption 2 (*Non-negativity*). $\mathcal{W}(\mathbf{X}; \mathbf{Y}) \geq 0$ and $\mathcal{M}(\mathbf{X}; \mathbf{Y}) \geq 0$.

Assumption 3 (*Existence*). For any $P \in \Delta$, there exists a Q^* that has pairwise distributions $Q(X_i, Y_j) = P(X_i, Y_j)$ and no high-order information, i.e. it has the same \mathcal{W} as P while satisfying $\mathcal{M} = 0$.

Assumption 1 formalises the intuition that low-order information consists of the “union” of all the pieces of information that any X_i holds about any Y_j . This requirement is theoretically supported [46] and follows from operational considerations from game theory [37] and information network theory [41]. This condition is also satisfied by many (though not all) commonly used measures of information decomposition [17, 37, 47, 48]. Assumption 2 is a desirable property of information decompositions in general, which greatly aids its interpretability¹ [17, 37]. Finally, Assumption 3 is less discussed in the literature, but it is a direct extension of Ref. [37].

Our first result is to show that these three assumptions determine \mathcal{W} and \mathcal{M} uniquely:

Proposition 1. *Under Assumptions 1-3, the \mathcal{W} - and \mathcal{M} -information between two random vectors \mathbf{X} and \mathbf{Y} assume a unique functional form given by*

$$\mathcal{W}(\mathbf{X}; \mathbf{Y}) = \min_{Q \in \Delta_P} I_Q(\mathbf{X}; \mathbf{Y}), \quad (3)$$

$$\mathcal{M}(\mathbf{X}; \mathbf{Y}) = I(\mathbf{X}; \mathbf{Y}) - \mathcal{W}(\mathbf{X}; \mathbf{Y}), \quad (4)$$

with $\Delta_P := \{Q \in \Delta : Q(X_i, Y_j) = P(X_i, Y_j) \forall i, j\}$ ².

Together, the expressions of \mathcal{W} - and \mathcal{M} -information above provide a principled way of decomposing the information shared between two random vectors into low-order (i.e. pairwise) and high-order (i.e. beyond-pairwise) components. Estimation techniques for these quantities are explored in the next section.

C. Calculating union and high-order information in Gaussian systems

While the minimisation in Eq. (3) is in general challenging, restricting the analysis to Gaussian \mathbf{X}, \mathbf{Y} allows us to prove the following two useful properties of \mathcal{W} :

Proposition 2. *Given \mathbf{X}, \mathbf{Y} multivariate jointly Gaussian random variables with non-singular marginal and cross-covariances, their \mathcal{W} -information is a convex function in the marginal covariances of \mathbf{X}, \mathbf{Y} .*

Proposition 3. *Given \mathbf{X}, \mathbf{Y} multivariate jointly Gaussian random variables with non-singular marginal covariances, the probability distribution Q^* that minimises Eq. (3) is an inner point of Δ_P .*

¹ Nonetheless, several measures do not satisfy this condition [49, 50] but are also theoretically justified [46].

² With a slight abuse of notation, we use the same symbol Δ_P as in Eq. (1). We consider this justified, as both definitions are the same (and equal to that of Refs. [37, 38]) when $d_Y = 1$.

With these results at hand, we can then state our main theorem, which enables us to design an efficient algorithm for computing \mathcal{W} :

Theorem 1. *The minimisation of Eq. (3) for the computation of \mathcal{W} -information can be solved via convex optimisation, and admits a unique solution $Q^* \in \Delta_P$.*

Proof. Direct from Propositions 2-3, and the fact that Δ_P is a convex set (see Appendix). \square

Thanks to Theorem 1, the \mathcal{W} -information can be efficiently calculated using standard tools from convex optimization [51, 52]. In the following, we provide an efficient unconstrained parametrisation for the feasible set Δ_P and perform the optimisation for \mathcal{W} -information. A complete technical description is provided in the Appendix.

Consider the joint Gaussian distribution $P(\mathbf{X}, \mathbf{Y})$ with zero mean and full-rank covariance Σ , and let L be its Cholesky decomposition, i.e. $\Sigma = LL^\top$. Using a block matrix representation, we can write:

$$\begin{aligned} \Sigma &= \begin{pmatrix} \Sigma_{XX} & \Sigma_{XY} \\ \Sigma_{YX} & \Sigma_{YY} \end{pmatrix} \\ &= LL^\top = \begin{pmatrix} L_{XX} & 0 \\ L_{YX} & L_{YY} \end{pmatrix} \begin{pmatrix} L_{XX}^\top & L_{YX}^\top \\ 0 & L_{YY}^\top \end{pmatrix} = \begin{pmatrix} L_{XX}L_{XX}^\top & L_{XX}L_{YX}^\top \\ L_{YX}L_{XX}^\top & L_{YX}L_{YX}^\top + L_{YY}L_{YY}^\top \end{pmatrix}, \end{aligned} \quad (5)$$

where $\Sigma_{XY} = \Sigma_{YX}^\top$, L_{XX} and L_{YY} are lower-triangular diagonal-positive matrices, and L_{YX} is any real matrix.

The constraint defining the optimisation set Δ_P requires that $\Sigma_{YX}^Q = \Sigma_{YX}$, with Q denoting the covariance of the optimised distribution. Enforcing this condition in Eq. (5), we obtain that the covariance matrix of a distribution $Q \in \Delta_P$ can be written as

$$\Sigma^Q = L^Q L^{Q,\top}, \quad \text{with} \quad L^Q = \begin{pmatrix} L_{XX}^Q & 0 \\ \Sigma_{YX}(L_{XX}^Q)^\top & L_{YY}^Q \end{pmatrix}, \quad (6)$$

where L_{XX}^Q and L_{YY}^Q are any lower triangular matrices³. Finally, we can parametrise L_{XX}^Q and L_{YY}^Q using a vector of real numbers, employing techniques from the Parametrization Cookbook [53].

Thus, following this procedure, the original constrained optimisation over the space of covariance matrices is reformulated as an unconstrained problem over the real numbers. Since all mappings involved are differentiable, the optimisation can be performed using standard gradient-based methods. In this work, all optimisations were performed using Adam [54].

III. RESULTS

A. Validation on synthetic data

a. Experiment 1: Toy systems. We start by calculating $\mathcal{W}(\mathbf{Z}_t; \mathbf{Z}_{t+1})$ and $\mathcal{M}(\mathbf{Z}_t; \mathbf{Z}_{t+1})$ for bivariate systems $\mathbf{Z}_t = (Z_t^1, Z_t^2)$ for which we have clear intuitions. We consider three scenarios: a ‘COPY’ system, where Z_t^i is coupled to Z_{t+1}^i ; a ‘transfer’ system, where Z_t^i is coupled to Z_{t+1}^j ($i \neq j$); and a Gaussian analogue to the XOR gate, which we expect to show high-order information (Fig. 1a; see Appendix for a full description). Results show that the decomposition of the input-output information is effectively decomposed into \mathcal{M} and \mathcal{W} , with the \mathcal{M} -information only assigning high-order components to the XOR gate. We remark that the small (unexpected) contributions of \mathcal{M} - and \mathcal{W} -information in COPY and XOR, respectively, are caused by numerical artefacts due to the input covariances being close to singular.

³ The constraints in Δ_P also require that $\text{diag}(\Sigma^P) = \text{diag}(\Sigma^Q)$. We address this in the Appendix.

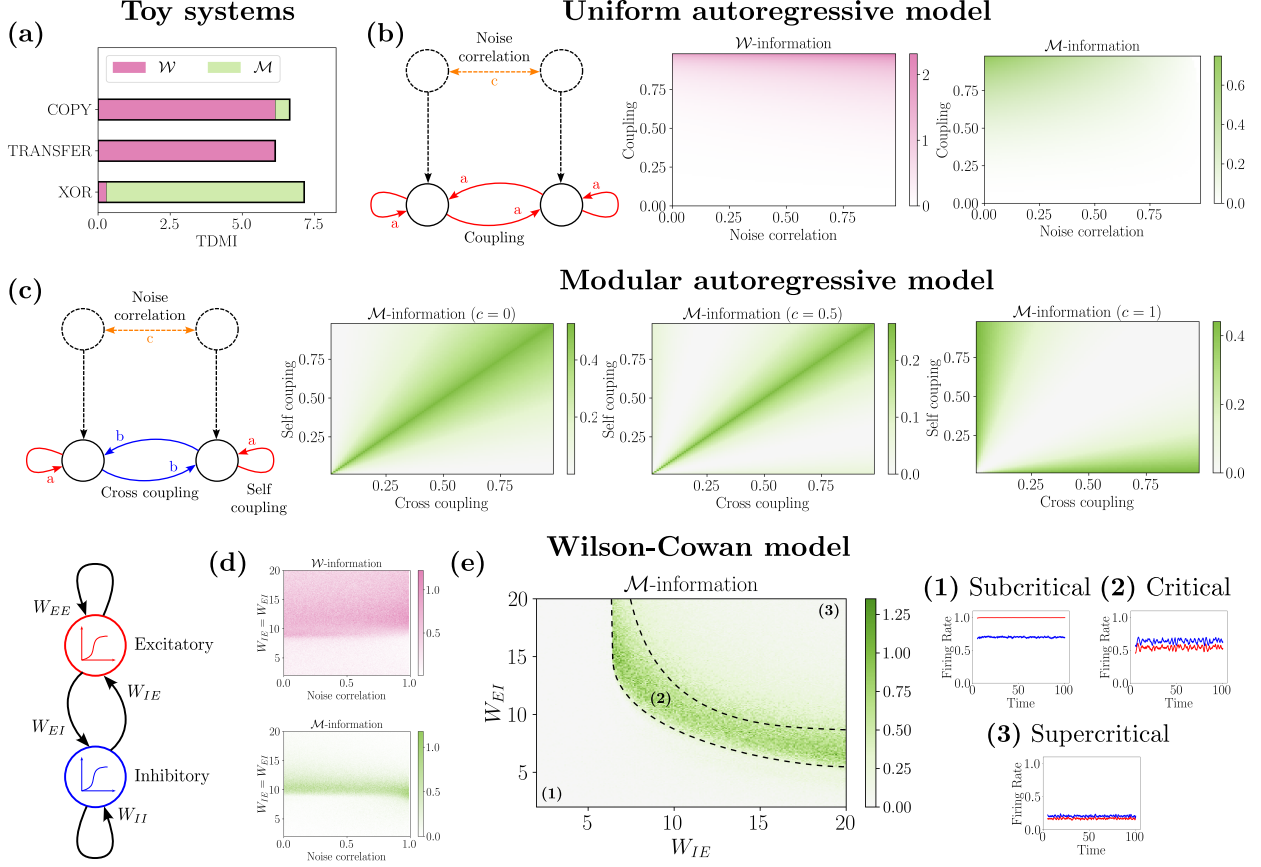


FIG. 1: \mathcal{M} -information captures high-order structures in linear and non-linear systems. (a) Computation of \mathcal{W} - and \mathcal{M} -information on COPY, Transfer, and XOR Gaussian systems shows that, as expected, only the XOR contains high-order information. (b) The uniform VAR model of Eq. (8) exhibits the highest \mathcal{W} -information for high coupling and noise correlation ($a \rightarrow 1$, $c \rightarrow 1$), and the highest \mathcal{M} -information for large coupling and low noise correlation ($a \rightarrow 1$, $c \rightarrow 1$). (c) For a VAR with modular interaction terms (Eq. (9)), \mathcal{M} -information is maximum for equal coefficients when the noise correlation is low ($a \approx b$, $c \lesssim 0.5$, and for uneven coefficients when the noise correlation is high. (d) In the Wilson-Cowan model, the estimation of \mathcal{W} and \mathcal{W} -information is robust to the injection of noise correlation dynamics in the system. (e) \mathcal{M} -information identifies 3 distinct regions in the phase space of the Wilson-Cowan dynamics, being highest in the critical regime.

b. Experiment 2: Uniform autoregressive process. We continue with the validation of the method by considering different Vector Autoregressive (VAR) systems on which we calculate \mathcal{W} - and \mathcal{M} -information. Specifically, given a VAR model

$$\mathbf{Z}_{t+1} = A\mathbf{Z}_t + \boldsymbol{\varepsilon}_t, \quad (7)$$

with $\mathbf{Z} = (Z^1, \dots, Z^n)$, $\boldsymbol{\varepsilon}_t \sim \mathcal{N}(0, V)$, setting different parameters A, V allows us to study how different dynamics are captured by \mathcal{W} . Here we show the case $n = 2$, but similar results hold for larger systems (see Appendix).

As above, we calculate $\mathcal{W}(\mathbf{Z}_t; \mathbf{Z}_{t+1})$ and $\mathcal{M}(\mathbf{Z}_t; \mathbf{Z}_{t+1})$, effectively analysing how information is integrated over time by the dynamics of the system. We start with a VAR model with parameters

$$A = \frac{1}{2} \begin{pmatrix} a & a \\ a & a \end{pmatrix} \quad \text{and} \quad V = \begin{pmatrix} 1 & c \\ c & 1 \end{pmatrix}, \quad (8)$$

with $a, c \in (-1, 1)$, so that the spectral radius of A is 1 when $a = 1$. Calculating \mathcal{M} - and \mathcal{W} -information for various values of (a, c) yields intuitive results (Fig. 1b): \mathcal{W} grows as c approaches 1 and the system is

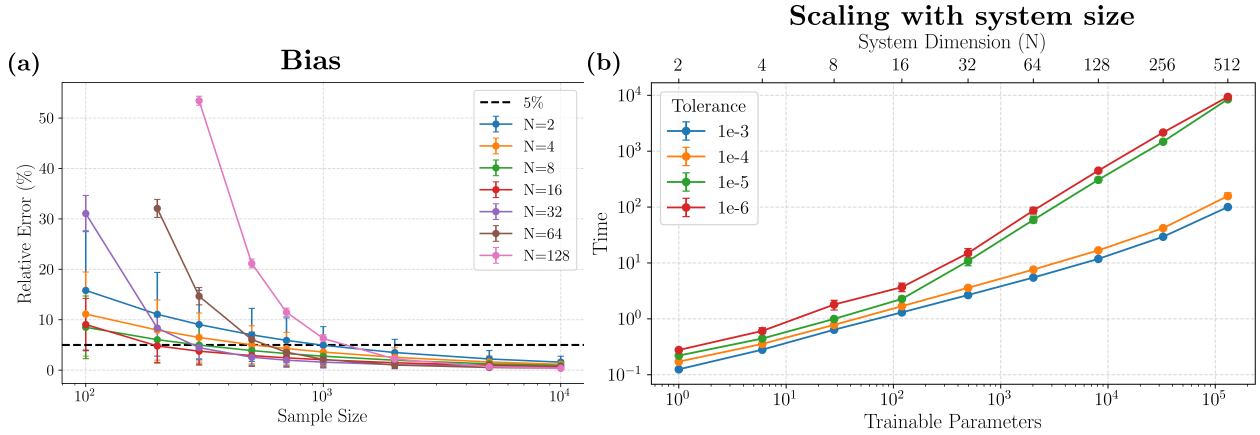


FIG. 2: The estimation of \mathcal{W} -information is accurate to within a few percentages, and its computation time scales efficiently with the system size. (a) Relative percentage accuracy of \mathcal{W} -information for different sample sizes and system dimensions. (b) Computational time in terms of trainable parameters of the system and system dimensions. Tolerances specify the convergence thresholds used in the optimisation. Error bars indicate the SEM.

more redundant; and \mathcal{M} is highest when all system elements are tightly coupled ($a \rightarrow 1$) and the noise is uncorrelated ($c \rightarrow 0$), effectively capturing dynamical cooperation not mediated by noise.

c. Experiment 3: Modular autoregressive process. To further study the interplay between dynamics and \mathcal{M} -information, we consider a VAR of the form:

$$A = \begin{pmatrix} a & b \\ b & a \end{pmatrix} \quad \text{and} \quad V = \begin{pmatrix} 1 & c \\ c & 1 \end{pmatrix}, \quad (9)$$

with $a, b, c \in (-1, 1)$. Fixing the parameter c , we perform an analogous analysis as before by varying a, b and calculating \mathcal{M} and \mathcal{W} . To facilitate comparison across the different systems, for each pair of (a, b) we rescale the spectral radius of A so that the system always possesses the same mutual information $I(\mathbf{Z}_t; \mathbf{Z}_{t+1})$. This ensures that differences in \mathcal{M} - and \mathcal{W} -information are only due to the internal dynamical structure of the model, and not to the total information content [55]. For low c , as expected, \mathcal{M} is high only when both self and cross coupling are high, as neither of them alone explains the dynamics of the system (Fig. 1c). Interestingly, this pattern is reversed for high c , plausibly because the asymmetry in the interactions (either high self and low cross coupling, or vice-versa) overcomes the effect of noise redundantly correlating the sources.

d. Experiment 4: Non-linear neural dynamics. Although the algorithm presented above was derived for Gaussian variables, we show that, in practice, our estimation of high-order interdependencies can be useful in more general (non-linear) cases. As an example, we consider a Wilson-Cowan (WC) model of interacting excitatory and inhibitory neuronal populations with non-linear gain functions, and analyse its information dynamics in different dynamical regimes.

We estimate the \mathcal{M} -information by fitting a Gaussian copula to the simulated steady-state distributions of neuronal activity, and employ the optimisation technique presented in Sec. II C across a range of excitatory-inhibitory (W_{EI}) and inhibitory-excitatory (W_{IE}) weights, as well as different values of the noise correlation c . We observe that \mathcal{M} -information delineates a specific region of high-order dependencies, which interestingly corresponds to the critical regime of sustained periodic oscillations (Fig. 1e). Furthermore, sweeping over various values of c shows that the \mathcal{M} -information is robust to noise (Fig. 1d). In sum, we show that \mathcal{M} -information is sensitive to biophysically meaningful modes of non-linear neural activity.

B. Bias correction and scalability

We now study how the accuracy and computational time of our method scale with system size. We test the former by sampling a random covariance matrix from a Wishart distribution, generating data of arbitrary

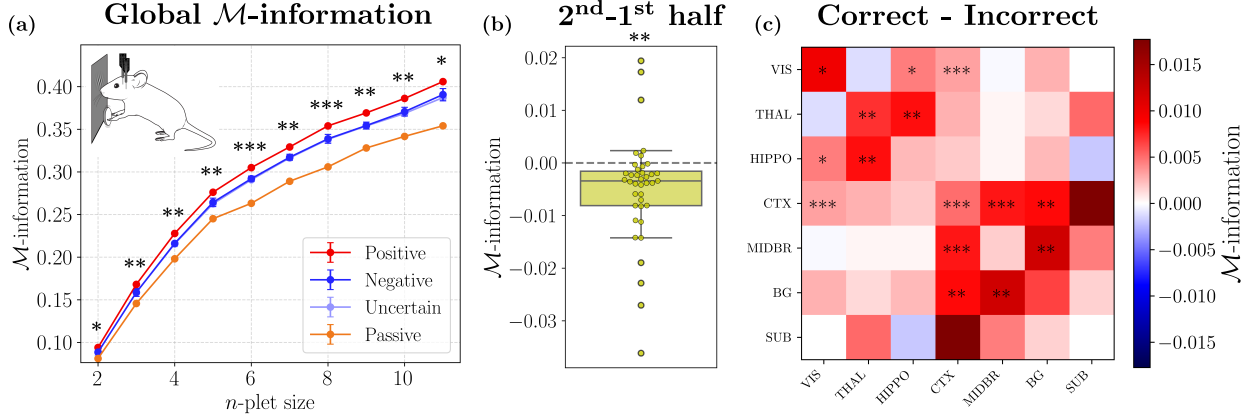


FIG. 3: \mathcal{M} -information in mouse neural activity captures perceptual performance in a visual discrimination task (a) \mathcal{M} -information of different trials across different n -plets sizes. Significance tests were performed between positive and negative trials. Error bars indicate the SEM. (b) Difference of \mathcal{M} -information between the second and first half of all active trials. (c) Difference of \mathcal{M} -information between correct and incorrect trials per regional interaction. All the \mathcal{M} -information values above are normalised w.r.t. to the mutual information. (P-values calculated with a one-sample t-test against the zero-mean null hypothesis. *: $p < 0.05$; **: $p < 0.01$; ***: $p < 0.001$).

length L , and estimating again the covariance of the system. Finally, we calculate \mathcal{W} -information and apply the bias correction suggested by Venkatesh *et al.* [40] (Fig. 2a). For smaller systems, the estimation error swiftly falls beneath the 5% threshold, and even for larger systems the bias falls within an acceptable range with approximately 1,000 samples. This makes it feasible to obtain accurate results on data such as fMRI [56], which typically consists of a few hundred time points and is known to pose challenges due to short time series and poor temporal resolution. Finally, we notice that \mathcal{W} -information calculated on a sample size of 10,000 provides an error below 1% for all system sizes studied here.

We then test the computational speed of our method on randomly sampled covariance matrices from Wishart distributions, showing that the optimisation scales efficiently with the system size and sub-linearly with the trainable parameters of the model (Fig. 2b). Overall, we find that the estimation of \mathcal{W} -information– and therefore of \mathcal{M} -information– is accurate, robust to different sampling sizes, and computationally efficient.

C. Empirical application: Mouse brain

We finally apply our measures of \mathcal{W} - and \mathcal{M} -information to a neuroimaging dataset of mice performing a visual discrimination task [57]. The dataset includes high-frequency local field potential (LFP) recordings from different brain regions while contrasting visual stimuli were presented on either side of a screen. Mice were trained to rotate a wheel to bring the high-contrast image towards the centre of the screen, with trials classified as positive (correct) or negative (incorrect) based on the accuracy of the choice. In certain trials where stimuli with equal contrast were presented on both sides, mice were randomly rewarded, and we refer to these trials as uncertain trials. Finally, as a control for stimulus presence, passive trials were performed where visual stimuli were presented with no instruction or reward. For each mouse and experimental session, multiple Neuropixel probes were placed across the brain to provide broad coverage of cortical and subcortical structures. We employed \mathcal{M} -information to assess the presence of high-order information structures during different trials, across various brain regions, and throughout the recording session. Since \mathcal{W} -information provides analogous results but from the low-order perspective, we report those findings in the Appendix.

We first apply \mathcal{M} -information to n -plets of neural populations, with $n \in [2, 11]$ (depending upon the recording session) in each of the four conditions. We observe that population activity has the highest \mathcal{M} -information when the mouse makes correct perceptual decisions, and the lowest \mathcal{M} -information when remaining passive. Stronger effects were obtained for larger n -plets, underscoring the importance of multivariate measures for accurately discriminating system behaviour (Fig. 3a). By computing \mathcal{M} -information on the first and second half of the trials in each run per each pair of pixels, we observe a decrease in \mathcal{M} over time (Fig. 3b).

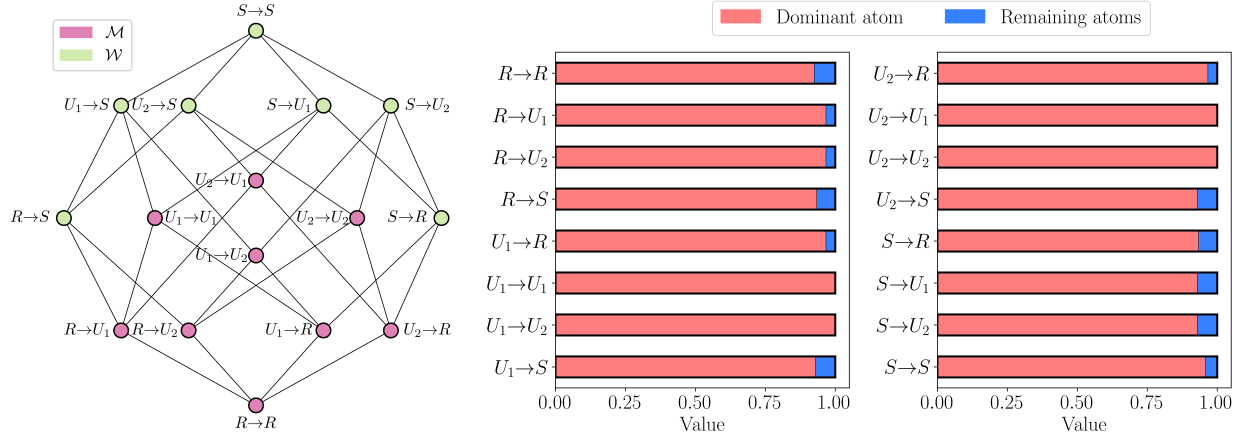


FIG. 4: BROJA- Φ ID successfully characterises information flow in toy systems. (a) Components of Φ ID arranged in a lattice, with terms highlighted according to their role in \mathcal{W} - and \mathcal{M} -information. (b) BROJA- Φ ID results on toy systems which are expected to have one dominant atom (reported on the y axis, red). The sum of all remaining atoms in each case is shown in blue.

This suggests that perceptual performance is initially subserved by distributed cooperation via macroscopic information processing, but once the mouse has accommodated to the task, computation is offloaded to low-order elements.

To gain greater neuroscientific insight into the biological orchestration of visual perception, we examine potential high-order interactions within and between specific anatomical areas (Fig. 3c). Comparing correct and incorrect perceptual decisions, we find a profound effect of increased high-order interactions within the neocortex, as well as between the neocortex and midbrain, basal ganglia, and visual cortex, respectively. We also observe significant increases for hippocampo-visual and thalamo-hippocampal interactions, likely reflecting the successful coordination of sensory variables with contextual memory and task-relevant information. Intriguingly, however, we do not find a significant effect for increased thalamo-visual interactions, which may be a consequence of the functional and cytoarchitectural heterogeneity of thalamic nuclei (see Appendix). Notably, we also observe greater \mathcal{M} -information within the visual cortex, as well as within the thalamus, indicating they function greater as wholes, rather than parts, during perceptual processing. In conclusion, \mathcal{M} -information reveals novel effects for the informational organisation of mammalian brains encoding behaviourally relevant variables.

IV. INFORMATION DECOMPOSITION BASED ON \mathcal{W} -INFORMATION

Having established that \mathcal{W} - and \mathcal{M} -information are meaningful measures in their own right, we finally show that the methodology developed above can be integrated with existing information-theoretic frameworks.

Part of the original motivation for the works in Refs. [37, 38] was to decompose mutual information using the Partial Information Decomposition (PID) framework [17]. PID aims to separate the the total information the sources \mathbf{X} have about the target Y into redundant, unique, and synergistic components, disentangling the amount of information shared by all sources, unique to each of them, and that arises only from their joint cooperation (respectively). In the case of two sources X_1, X_2 and a target Y , PID states that marginal and joint mutual information can be written as

$$I(X_1; Y) = R + U_1 \quad (10a)$$

$$I(X_2; Y) = R + U_2 \quad (10b)$$

$$I(X_1, X_2; Y) = R + U_1 + U_2 + S, \quad (10c)$$

where R represents redundancy, U_1, U_2 unique information of X_1, X_2 , respectively, and S synergy. Importantly, these equations do not define a unique functional form for R, U_i and S , and many different approaches have been proposed [17, 38, 47–50, 58–62].

However, despite its flexibility, the PID formalism does not enable a decomposition of multivariate targets. Therefore, a generalisation of PID to multiple targets has been proposed under the name of Integrated Information Decomposition (Φ ID) [35, 63]. Φ ID decomposes the mutual information between two channels into R , U , and S components both in sources and targets, providing a finer-grained decomposition of mutual information. As an example, information that is redundant in the sources and unique to one target would be denoted $R \rightarrow U_1$, and similarly for all other components.

Calculating Φ ID requires a choice of PID and an additional condition. For the former, we adopt the BROJA-PID [37]; for the latter, we argue that all the low-order components should only depend on redundancy and unique information terms, and should therefore be included in the \mathcal{W} -information. This provides the following additional constraint:

$$\begin{aligned} \mathcal{W} = & R \rightarrow R + R \rightarrow U_1 + R \rightarrow U_2 + \\ & U_1 \rightarrow R + U_1 \rightarrow U_1 + U_1 \rightarrow U_2 + \\ & U_2 \rightarrow R + U_2 \rightarrow U_1 + U_2 \rightarrow U_2 \quad . \end{aligned} \quad (11)$$

Hence, with Eq. (11) and the BROJA-PID at hand, we can perform the full Φ ID decomposition of the system. We name this approach BROJA- Φ ID. See the Appendix for details.

To validate our proposed decomposition, we analyse again the toy models considered in Sec. III, but here designed to maximise a specific Φ ID atom (Fig. 4a). Indeed, we find that in all cases, BROJA- Φ ID assigns the dominant contribution to the correct atom, proving its ability to discriminate among different types of integration dynamics. Hence, not only is it possible to assess the total high-order information via \mathcal{M} -information, but also to uncover which specific information atoms are responsible for it via BROJA- Φ ID.

V. RELATED WORK

a. High-order measures. A great number of high-order information measures exist in the literature, which include (among others) the interaction information [64–67], the Delta-information [68, 69], the O-information [34], the redundancy-synergy index [32], Varadan’s synergy [70], information decomposition approaches [17], and measures aimed at quantifying emergent behaviour [71–73]. A separate, prominent line of work quantifying high-order information in dynamical systems is integrated information theory [33, 74] within which multiple measures are available [75], including some based on information decomposition [63] and information geometry [76, 77].

b. Information decomposition. Among the many high-order information measures, information decomposition approaches play a fundamental role due to their ability to disentangle distinct modes of information sharing. The seminal work of Williams and Beer introduced the framework of Partial Information Decomposition (PID), in which the mutual information between an arbitrary number of sources and a single target is divided into redundant, unique, and synergistic terms [17]. Following this work, many different PID formulations have been suggested [17, 38, 47–50, 58–62], including the BROJA definition proposed contemporaneously by Bertschinger *et al.* [37] and Griffith and Koch [38], which forms the inspiration of this work. Ince introduced an entropy-based decomposition [78, 79], Varley a Kullback-Leibler divergence decomposition [80], and Mediano *et al.* generalised PID by decomposing both information from sources and targets symmetrically [63].

c. Algorithms for information optimisation. Various algorithms have been previously introduced to improve the computation of PID quantities, as well as information quantities more broadly. Makkeh *et al.* proposed a refinement of the original BROJA-PID optimisation for the discrete case via cone programming [43], while Venkatesh *et al.* improved it for Gaussian variables using projected gradient descent [40]. Kleinman *et al.* [81] proposed a measure of redundant information based on the result of a learning problem. Inspired by PID, McSharry *et al.* [82, 83] proposed a representation learning architecture to learn highly synergistic features from data. More generally, there is a wide range of variational methods that turn the estimation of mutual information into an optimisation problem [84].

VI. CONCLUSION

a. Summary of findings. We introduced the \mathcal{W} - and \mathcal{M} -information, novel information-theoretic measures of low- and high-order information structure, tailored for use on large dynamical systems. In addition to formulating the calculation of \mathcal{W} as a convex optimisation problem, we designed a robust and efficient algorithm that enables practical applications to large, high-dimensional systems. We illustrated their behaviour on synthetic systems with Gaussian and non-linear dynamics, showing them to be robust to noise and capable of indexing critical behaviour. Finally, we employed \mathcal{M} -information to analyse empirical brain activity data of mice during a visual discrimination task, showing that higher values of \mathcal{M} -information reflect accurate perceptual performance – hence demonstrating that \mathcal{M} and \mathcal{W} can detect meaningful phenomena in real-world scenarios. Moreover, as an additional theoretical contribution, we provided an information decomposition framework based on \mathcal{W} - and \mathcal{M} -information, enabling a finer-grained analysis of multivariate information dynamics.

b. Limitations and future work. Although \mathcal{W} -information is defined for any probability distribution, here we have focused only on the case where \mathbf{X}, \mathbf{Y} are jointly Gaussian. To compute \mathcal{W} in other scenarios, and potentially make calculations in the Gaussian case faster, future works could design more efficient optimisers that make better use of the geometry of Δ_P via Riemannian machine learning [85] or generalise to other distributions [45]. Finally, \mathcal{W} and \mathcal{M} could contribute to the promising recent line of work using information decomposition as an objective function for learning in deep learning systems [86].

c. Final remarks. We demonstrated that \mathcal{M} -information is a powerful estimator of high-order information, which stands on solid mathematical and operational grounds [37, 38, 41], and whose efficient computational scalability enables broad applicability across diverse real-world domains, in neuroscience and beyond. By bridging principled information-theoretic foundations with practical feasibility, \mathcal{M} -information opens the door to a new generation of tools for quantifying collective interactions in high-dimensional complex systems.

ACKNOWLEDGEMENTS

We thank Maximilian Kathofer for useful discussions.

CODE AVAILABILITY

The Python code for calculating \mathcal{W} -, \mathcal{M} -information, and BROJA- Φ ID is publicly available and can be found at <https://github.com/alberto-liardi/wimfo>.

-
- [1] G. Tononi, G. M. Edelman, and O. Sporns, “Complexity and coherency: integrating information in the brain,” *Trends in cognitive sciences*, vol. 2, no. 12, pp. 474–484, 1998.
 - [2] G. Buzsáki, *Rhythms of the Brain*. Oxford university press, 2006.
 - [3] K. Friston, “The free-energy principle: a unified brain theory?,” *Nature reviews neuroscience*, vol. 11, no. 2, pp. 127–138, 2010.
 - [4] D. S. Bassett and M. S. Gazzaniga, “Understanding complexity in the human brain,” *Trends in cognitive sciences*, vol. 15, no. 5, pp. 200–209, 2011.
 - [5] Y. LeCun, Y. Bengio, and G. Hinton, “Deep learning,” *nature*, vol. 521, no. 7553, pp. 436–444, 2015.
 - [6] D. Hassabis, D. Kumaran, C. Summerfield, and M. Botvinick, “Neuroscience-inspired artificial intelligence,” *Neuron*, vol. 95, no. 2, pp. 245–258, 2017.
 - [7] M. Raghu and E. Schmidt, “A survey of deep learning for scientific discovery,” *arXiv preprint arXiv:2003.11755*, 2020.
 - [8] F. E. Rosas, P. A. Mediano, A. I. Luppi, T. F. Varley, J. T. Lizier, S. Stramaglia, H. J. Jensen, and D. Marinazzo, “Disentangling high-order mechanisms and high-order behaviours in complex systems,” *Nature Physics*, vol. 18, no. 5, pp. 476–477, 2022.
 - [9] H. J. Morowitz, *The emergence of everything: How the world became complex*. Oxford University Press, 2002.
 - [10] A. I. Luppi, F. E. Rosas, P. A. Mediano, D. K. Menon, and E. A. Stamatakis, “Information decomposition and the informational architecture of the brain,” *Trends in Cognitive Sciences*, 2024.

- [11] E. Schneidman, M. J. Berry, R. Segev, and W. Bialek, “Weak pairwise correlations imply strongly correlated network states in a neural population,” *Nature*, vol. 440, no. 7087, pp. 1007–1012, 2006.
- [12] E. Ganmor, R. Segev, and E. Schneidman, “Sparse low-order interaction network underlies a highly correlated and learnable neural population code,” *Proceedings of the National Academy of sciences*, vol. 108, no. 23, pp. 9679–9684, 2011.
- [13] S. Yu, H. Yang, H. Nakahara, G. S. Santos, D. Nikolić, and D. Plenz, “Higher-order interactions characterized in cortical activity,” *Journal of neuroscience*, vol. 31, no. 48, pp. 17514–17526, 2011.
- [14] C. Giusti, E. Pastalkova, C. Curto, and V. Itskov, “Cliques topology reveals intrinsic geometric structure in neural correlations,” *Proceedings of the National Academy of Sciences*, vol. 112, no. 44, pp. 13455–13460, 2015.
- [15] A. E. Sizemore, C. Giusti, A. Kahn, J. M. Vettel, R. F. Betzel, and D. S. Bassett, “Cliques and cavities in the human connectome,” *Journal of computational neuroscience*, vol. 44, pp. 115–145, 2018.
- [16] G. Petri, P. Expert, F. Turkheimer, R. Carhart-Harris, D. Nutt, P. J. Hellyer, and F. Vaccarino, “Homological scaffolds of brain functional networks,” *Journal of The Royal Society Interface*, vol. 11, no. 101, p. 20140873, 2014.
- [17] P. L. Williams and R. D. Beer, “Nonnegative decomposition of multivariate information,” *arXiv preprint arXiv:1004.2515*, 2010.
- [18] N. M. Timme, S. Ito, M. Myroshnychenko, S. Nigam, M. Shimono, F.-C. Yeh, P. Hottowy, A. M. Litke, and J. M. Beggs, “High-degree neurons feed cortical computations,” *PLoS computational biology*, vol. 12, no. 5, p. e1004858, 2016.
- [19] P. A. Mediano, F. E. Rosas, A. I. Luppi, H. J. Jensen, A. K. Seth, A. B. Barrett, R. L. Carhart-Harris, and D. Bor, “Greater than the parts: A review of the information decomposition approach to causal emergence,” *Philosophical Transactions of the Royal Society A*, vol. 380, no. 2227, p. 20210246, 2022.
- [20] I. E. Ohiorhenuan, F. Mechler, K. P. Purpura, A. M. Schmid, Q. Hu, and J. D. Victor, “Sparse coding and high-order correlations in fine-scale cortical networks,” *Nature*, vol. 466, no. 7306, pp. 617–621, 2010.
- [21] H. Park, R. A. Ince, P. G. Schyngs, G. Thut, and J. Gross, “Representational interactions during audiovisual speech entrainment: Redundancy in left posterior superior temporal gyrus and synergy in left motor cortex,” *PLoS biology*, vol. 16, no. 8, p. e2006558, 2018.
- [22] G. Pica, E. Piasini, H. Safaai, C. Runyan, C. Harvey, M. Diamond, C. Kayser, T. Fellin, and S. Panzeri, “Quantifying how much sensory information in a neural code is relevant for behavior,” *Advances in Neural Information Processing Systems*, vol. 30, 2017.
- [23] T. F. Varley, O. Sporns, N. J. Stevenson, M. G. Welch, M. M. Myers, S. Vanhatalo, and A. Tokariev, “Emergence of a synergistic scaffold in the brains of human infants,” *bioRxiv*, pp. 2024–02, 2024.
- [24] M. Gatica, R. Cofré, P. A. Mediano, F. E. Rosas, P. Orio, I. Diez, S. P. Swinnen, and J. M. Cortes, “High-order interdependencies in the aging brain,” *Brain connectivity*, vol. 11, no. 9, pp. 734–744, 2021.
- [25] A. I. Luppi, P. A. Mediano, F. E. Rosas, J. Allanson, J. D. Pickard, G. B. Williams, M. M. Craig, P. Finoia, A. R. Peattie, P. Coppola, *et al.*, “Reduced emergent character of neural dynamics in patients with a disrupted connectome,” *NeuroImage*, vol. 269, p. 119926, 2023.
- [26] P. A. Mediano, F. E. Rosas, D. Bor, A. K. Seth, and A. B. Barrett, “The strength of weak integrated information theory,” *Trends in Cognitive Sciences*, vol. 26, no. 8, pp. 646–655, 2022.
- [27] A. M. Proca, F. E. Rosas, A. I. Luppi, D. Bor, M. Crosby, and P. A. Mediano, “Synergistic information supports modality integration and flexible learning in neural networks solving multiple tasks,” *PLOS Computational Biology*, vol. 20, no. 6, p. e1012178, 2024.
- [28] D. Sorokina, R. Caruana, M. Riedewald, and D. Fink, “Detecting statistical interactions with additive groves of trees,” in *Proceedings of the 25th international conference on Machine learning*, pp. 1000–1007, 2008.
- [29] M. Tsang, D. Cheng, and Y. Liu, “Detecting statistical interactions from neural network weights,” *arXiv preprint arXiv:1705.04977*, 2017.
- [30] D. A. Ehrlich, A. C. Schneider, V. Priesemann, M. Wibral, and A. Makkeh, “A measure of the complexity of neural representations based on partial information decomposition,” *Transactions on Machine Learning Research*, 2023.
- [31] A. J. Gutknecht, F. E. Rosas, D. A. Ehrlich, A. Makkeh, P. A. M. Mediano, and M. Wibral, “Shannon invariants: A scalable approach to information decomposition,” *arXiv preprint arXiv:2504.15779*, 2025.
- [32] G. Chechik, A. Globerson, M. Anderson, E. Young, I. Nelken, and N. Tishby, “Group redundancy measures reveal redundancy reduction in the auditory pathway,” *Advances in neural information processing systems*, vol. 14, 2001.
- [33] D. Balduzzi and G. Tononi, “Integrated information in discrete dynamical systems: motivation and theoretical framework,” *PLoS Computational Biology*, vol. 4, no. 6, p. e1000091, 2008.
- [34] F. Rosas, P. A. M. Mediano, M. Gastpar, and H. J. Jensen, “Quantifying high-order interdependencies via multivariate extensions of the mutual information,” vol. 100, no. 3, p. 032305.
- [35] P. A. Mediano, F. Rosas, R. L. Carhart-Harris, A. K. Seth, and A. B. Barrett, “Beyond integrated information: A taxonomy of information dynamics phenomena,” *arXiv preprint arXiv:1909.02297*, 2019.
- [36] F. Rosas, P. A. Mediano, M. Ugarte, and H. J. Jensen, “An information-theoretic approach to self-organisation: Emergence of complex interdependencies in coupled dynamical systems,” *Entropy*, vol. 20, no. 10, p. 793, 2018.

- [37] N. Bertschinger, J. Rauh, E. Olbrich, J. Jost, and N. Ay, “Quantifying unique information,” *Entropy*, vol. 16, no. 4, pp. 2161–2183, 2014.
- [38] V. Griffith and C. Koch, “Quantifying synergistic mutual information,” in *Guided self-organization: inception*, pp. 159–190, Springer, 2014.
- [39] R. G. James, C. J. Ellison, and J. P. Crutchfield, ““dit“: A Python package for discrete information theory,” *Journal of Open Source Software*, vol. 3, no. 25, p. 738, 2018.
- [40] P. Venkatesh, C. Bennett, S. Gale, T. Ramirez, G. Heller, S. Durand, S. Olsen, and S. Mihalas, “Gaussian partial information decomposition: Bias correction and application to high-dimensional data,” *Advances in Neural Information Processing Systems*, vol. 36, pp. 74602–74635, 2023.
- [41] C. Tian and S. Shamai, “Broadcast channel cooperative gain: An operational interpretation of partial information decomposition,” *Entropy*, vol. 27, no. 3, p. 310, 2025.
- [42] A. Kolchinsky, “A novel approach to the partial information decomposition,” *Entropy*, vol. 24, no. 3, p. 403, 2022.
- [43] A. Makkeh, D. O. Theis, and R. Vicente, “BROJA-2PID: A robust estimator for bivariate partial information decomposition,” *Entropy*, vol. 20, no. 4, p. 271, 2018.
- [44] P. Wollstadt, J. T. Lizier, R. Vicente, C. Finn, M. Martinez-Zarzuela, P. Mediano, L. Novelli, and M. Wibral, “IDTxL: The information dynamics toolkit xL: A Python package for the efficient analysis of multivariate information dynamics in networks,” *arXiv preprint arXiv:1807.10459*, 2018.
- [45] A. Pakman, A. Nejatbakhsh, D. Gilboa, A. Makkeh, L. Mazzucato, M. Wibral, and E. Schneidman, “Estimating the unique information of continuous variables,” *Advances in Neural Information Processing Systems*, vol. 34, pp. 20295–20307, 2021.
- [46] C. Finn and J. T. Lizier, “Pointwise partial information decomposition using the specificity and ambiguity lattices,” *Entropy*, vol. 20, no. 4, p. 297, 2018.
- [47] M. Harder, C. Salge, and D. Polani, “Bivariate measure of redundant information,” *Physical Review E*, vol. 87, no. 1, p. 012130, 2013.
- [48] A. B. Barrett, “Exploration of synergistic and redundant information sharing in static and dynamical gaussian systems,” *Physical Review E*, vol. 91, no. 5, p. 052802, 2015.
- [49] R. A. Ince, “Measuring multivariate redundant information with pointwise common change in surprisal,” *Entropy*, vol. 19, no. 7, p. 318, 2017.
- [50] F. E. Rosas, P. A. Mediano, B. Rassouli, and A. B. Barrett, “An operational information decomposition via synergistic disclosure,” *Journal of Physics A: Mathematical and Theoretical*, vol. 53, no. 48, p. 485001, 2020.
- [51] S. P. Boyd and L. Vandenberghe, *Convex optimization*. Cambridge university press, 2004.
- [52] A. W. Marshall, I. Olkin, and B. C. Arnold, “Inequalities: theory of majorization and its applications,” 1979.
- [53] J.-B. Leger, “Parametrization cookbook: A set of bijective parametrizations for using machine learning methods in statistical inference,” *arXiv preprint arXiv:2301.08297*, 2023.
- [54] D. P. Kingma, “Adam: A method for stochastic optimization,” *arXiv preprint arXiv:1412.6980*, 2014.
- [55] A. Liardi, F. E. Rosas, R. L. Carhart-Harris, G. Blackburne, D. Bor, and P. A. Mediano, “Null models for comparing information decomposition across complex systems,” *arXiv preprint arXiv:2410.11583*, 2024.
- [56] D. C. Van Essen, K. Ugurbil, E. Auerbach, D. Barch, T. E. Behrens, R. Bucholz, A. Chang, L. Chen, M. Corbetta, S. W. Curtiss, *et al.*, “The human connectome project: a data acquisition perspective,” *Neuroimage*, vol. 62, no. 4, pp. 2222–2231, 2012.
- [57] N. A. Steinmetz, P. Zátka-Haas, M. Carandini, and K. D. Harris, “Distributed coding of choice, action and engagement across the mouse brain,” *Nature*, vol. 576, no. 7786, pp. 266–273, 2019.
- [58] N. Bertschinger, J. Rauh, E. Olbrich, and J. Jost, “Shared information—new insights and problems in decomposing information in complex systems,” in *Proceedings of the European conference on complex systems 2012*, pp. 251–269, Springer, 2013.
- [59] R. G. James, J. Emenheiser, and J. P. Crutchfield, “Unique information via dependency constraints,” *Journal of Physics A: Mathematical and Theoretical*, vol. 52, no. 1, p. 014002, 2018.
- [60] V. Griffith, E. K. Chong, R. G. James, C. J. Ellison, and J. P. Crutchfield, “Intersection information based on common randomness,” *Entropy*, vol. 16, no. 4, pp. 1985–2000, 2014.
- [61] V. Griffith and T. Ho, “Quantifying redundant information in predicting a target random variable,” *Entropy*, vol. 17, no. 7, pp. 4644–4653, 2015.
- [62] R. Quax, O. Har-Shemesh, and P. M. Sloom, “Quantifying synergistic information using intermediate stochastic variables,” *Entropy*, vol. 19, no. 2, p. 85, 2017.
- [63] P. A. Mediano, F. E. Rosas, A. I. Luppi, R. L. Carhart-Harris, D. Bor, A. K. Seth, and A. B. Barrett, “Towards an extended taxonomy of information dynamics via integrated information decomposition,” *arXiv preprint arXiv:2109.13186*, 2021.
- [64] I. Gat and N. Tishby, “Synergy and redundancy among brain cells of behaving monkeys,” *Advances in neural information processing systems*, vol. 11, 1998.
- [65] N. Brenner, S. P. Strong, R. Koberle, W. Bialek, and R. R. d. R. v. Steveninck, “Synergy in a neural code,” *Neural computation*, vol. 12, no. 7, pp. 1531–1552, 2000.
- [66] E. Schneidman, W. Bialek, and M. J. Berry, “Synergy, redundancy, and independence in population codes,” *Journal of Neuroscience*, vol. 23, no. 37, pp. 11539–11553, 2003.

- [67] D. Anastassiou, “Computational analysis of the synergy among multiple interacting genes,” *Molecular systems biology*, vol. 3, no. 1, p. 83, 2007.
- [68] S. Nirenberg, S. M. Carcieri, A. L. Jacobs, and P. E. Latham, “Retinal ganglion cells act largely as independent encoders,” *Nature*, vol. 411, no. 6838, pp. 698–701, 2001.
- [69] P. E. Latham and S. Nirenberg, “Synergy, redundancy, and independence in population codes, revisited,” *Journal of Neuroscience*, vol. 25, no. 21, pp. 5195–5206, 2005.
- [70] V. Varadan, D. M. Miller III, and D. Anastassiou, “Computational inference of the molecular logic for synaptic connectivity in *c. elegans*,” *Bioinformatics*, vol. 22, no. 14, pp. e497–e506, 2006.
- [71] F. E. Rosas, P. A. Mediano, H. J. Jensen, A. K. Seth, A. B. Barrett, R. L. Carhart-Harris, and D. Bor, “Reconciling emergences: An information-theoretic approach to identify causal emergence in multivariate data,” *PLoS Computational Biology*, vol. 16, no. 12, p. e1008289, 2020.
- [72] L. Barnett and A. K. Seth, “Dynamical independence: discovering emergent macroscopic processes in complex dynamical systems,” *Physical Review E*, vol. 108, no. 1, p. 014304, 2023.
- [73] F. E. Rosas, B. C. Geiger, A. I. Luppi, A. K. Seth, D. Polani, M. Gastpar, and P. A. Mediano, “Software in the natural world: A computational approach to emergence in complex multi-level systems,” *arXiv preprint arXiv:2402.09090*, 2024.
- [74] M. Oizumi, L. Albantakis, and G. Tononi, “From the phenomenology to the mechanisms of consciousness: Integrated information theory 3.0,” *PLoS Computational Biology*, vol. 10, no. 5, p. e1003588, 2014.
- [75] P. A. Mediano, A. K. Seth, and A. B. Barrett, “Measuring integrated information: Comparison of candidate measures in theory and simulation,” *Entropy*, vol. 21, no. 1, p. 17, 2018.
- [76] M. Oizumi, N. Tsuchiya, and S.-i. Amari, “Unified framework for information integration based on information geometry,” *Proceedings of the National Academy of Sciences*, vol. 113, no. 51, pp. 14817–14822, 2016.
- [77] C. Langer and N. Ay, “Complexity as causal information integration,” *Entropy*, vol. 22, no. 10, p. 1107, 2020.
- [78] R. A. Ince, “The partial entropy decomposition: Decomposing multivariate entropy and mutual information via pointwise common surprisal,” *arXiv preprint arXiv:1702.01591*, 2017.
- [79] T. F. Varley, M. Pope, M. Grazia, Joshua, and O. Sporns, “Partial entropy decomposition reveals higher-order information structures in human brain activity,” *Proceedings of the National Academy of Sciences*, vol. 120, no. 30, p. e2300888120, 2023.
- [80] T. F. Varley, “Generalized decomposition of multivariate information,” *Plos One*, vol. 19, no. 2, p. e0297128, 2024.
- [81] M. Kleinman, A. Achille, S. Soatto, and J. C. Kao, “Redundant information neural estimation,” *Entropy*, vol. 23, no. 7, p. 922, 2021.
- [82] D. McSharry, C. Kaplanis, F. Rosas, and P. A. Mediano, “Learning diverse causally emergent representations from time series data,” *Advances in Neural Information Processing Systems*, vol. 37, pp. 119547–119572, 2024.
- [83] C. Kaplanis, P. Mediano, and F. Rosas, “Learning causally emergent representations,” in *NeurIPS 2023 workshop: Information-Theoretic Principles in Cognitive Systems*, 2023.
- [84] B. Poole, S. Ozair, A. Van Den Oord, A. Alemi, and G. Tucker, “On variational bounds of mutual information,” in *International Conference on Machine Learning*, pp. 5171–5180, PMLR, 2019.
- [85] M. Kochurov, R. Karimov, and S. Kozlukov, “Geoopt: Riemannian optimization in PyTorch,” 2020.
- [86] A. Makkeh, M. Graetz, A. C. Schneider, D. A. Ehrlich, V. Priesemann, and M. Wibral, “A general framework for interpretable neural learning based on local information-theoretic goal functions,” *Proceedings of the National Academy of Sciences*, vol. 122, no. 10, p. e2408125122, 2025.
- [87] T. M. Cover and J. A. Thomas, *Elements of Information Theory*. John Wiley & Sons, 1999.
- [88] T. M. Cover and J. A. Thomas, “Information theory and the stock market,” *Elements of Information Theory*. Wiley Inc., New York, pp. 543–556, 1991.
- [89] R. A. Horn and C. R. Johnson, *Matrix analysis*. Cambridge University Press, 2012.
- [90] R. Bhatia, *Positive definite matrices*. Princeton University Press, 2009.
- [91] K. B. Petersen, M. S. Pedersen, *et al.*, “The matrix cookbook,” *Technical University of Denmark*, vol. 7, no. 15, p. 510, 2008.
- [92] F. Zhang, *The Schur complement and its applications*, vol. 4. Springer Science & Business Media, 2006.
- [93] J. M. Box-Steffensmeier, J. R. Freeman, M. P. Hitt, and J. C. Pevehouse, *Time series analysis for the social sciences*. Cambridge University Press, 2014.
- [94] C. A. Sims, “Macroeconomics and reality,” *Econometrica: journal of the Econometric Society*, pp. 1–48, 1980.
- [95] A. Hatemi-J, “Multivariate tests for autocorrelation in the stable and unstable var models,” *Economic Modelling*, vol. 21, no. 4, pp. 661–683, 2004.
- [96] A. B. Barrett, L. Barnett, and A. K. Seth, “Multivariate granger causality and generalized variance,” *Physical Review E*, vol. 81, no. 4, p. 041907, 2010.
- [97] G. E. Box, G. M. Jenkins, G. C. Reinsel, and G. M. Ljung, *Time series analysis: forecasting and control*. John Wiley & Sons, 2015.
- [98] G. U. Yule, “Vii. on a method of investigating periodicities disturbed series, with special reference to wolfer’s sunspot numbers,” *Philosophical Transactions of the Royal Society of London. Series A, Containing Papers of a Mathematical or Physical Character*, vol. 226, no. 636-646, pp. 267–298, 1927.

- [99] G. T. Walker, "On periodicity in series of related terms," *Proceedings of the Royal Society of London. Series A, Containing Papers of a Mathematical and Physical Character*, vol. 131, no. 818, pp. 518–532, 1931.
- [100] H. R. Wilson and J. D. Cowan, "Excitatory and inhibitory interactions in localized populations of model neurons," *Biophysical journal*, vol. 12, no. 1, pp. 1–24, 1972.
- [101] H. R. Wilson and J. D. Cowan, "A mathematical theory of the functional dynamics of cortical and thalamic nervous tissue," *Kybernetik*, vol. 13, no. 2, pp. 55–80, 1973.
- [102] T. Sejnowski, "On global properties of neuronal interaction," *Biological Cybernetics*, vol. 22, no. 2, pp. 85–95, 1976.
- [103] D. J. Amit and N. Brunel, "Model of global spontaneous activity and local structured activity during delay periods in the cerebral cortex," *Cerebral cortex (New York, NY: 1991)*, vol. 7, no. 3, pp. 237–252, 1997.
- [104] N. Brunel, "Dynamics of sparsely connected networks of excitatory and inhibitory spiking neurons," *Journal of computational neuroscience*, vol. 8, pp. 183–208, 2000.
- [105] A. Renart, R. Moreno-Bote, X.-J. Wang, and N. Parga, "Mean-driven and fluctuation-driven persistent activity in recurrent networks," *Neural computation*, vol. 19, no. 1, pp. 1–46, 2007.
- [106] M. Breakspear, "Dynamic models of large-scale brain activity," *Nature neuroscience*, vol. 20, no. 3, pp. 340–352, 2017.
- [107] A. Destexhe and T. J. Sejnowski, "The wilson–cowan model, 36 years later," *Biological cybernetics*, vol. 101, no. 1, pp. 1–2, 2009.
- [108] S. Coombes, "Waves, bumps, and patterns in neural field theories," *Biological cybernetics*, vol. 93, pp. 91–108, 2005.
- [109] B. Ermentrout and D. H. Terman, *Mathematical foundations of neuroscience*, vol. 35. Springer, 2010.
- [110] J. D. Cowan, J. Neuman, and W. van Drongelen, "Wilson–cowan equations for neocortical dynamics," *The Journal of Mathematical Neuroscience*, vol. 6, pp. 1–24, 2016.
- [111] R. A. Ince, B. L. Giordano, C. Kayser, G. A. Rousselet, J. Gross, and P. G. Schyns, "A statistical framework for neuroimaging data analysis based on mutual information estimated via a gaussian copula," *Human brain mapping*, vol. 38, no. 3, pp. 1541–1573, 2017.

Appendix A: Optimisation algorithm for \mathcal{W} -information

Here we describe in full detail the optimisation procedure implemented for the calculation of \mathcal{W} -information.

Let's consider a joint system (\mathbf{X}, \mathbf{Y}) that follows a Gaussian distribution with full-rank covariance Σ . We denote by P the original distribution of the system, and by Q the distribution being optimised. To differentiate between the two, we use superscripts: quantities referring to Q will carry a superscript (e.g. Σ^Q), while those associated with the original distribution P will be written without any (e.g. Σ).

Given the domain Δ_P that contains all probability distributions Q such that $Q(X_i, Y_j) = P(X_i, Y_j)$, we remind that the objective of the optimisation is to find the distribution $Q^* \in \Delta_P$ that minimises the mutual information $I_Q(\mathbf{X}, \mathbf{Y})$. For Gaussian variables, this has the form:

$$I_Q(\mathbf{X}, \mathbf{Y}) = \frac{1}{2} \log \left(\frac{\det(\Sigma_X^Q) \det(\Sigma_Y^Q)}{\det(\Sigma^Q)} \right). \quad (\text{A1})$$

Therefore, we look for a convenient parametrisation of the covariance matrices of the probability distributions in Δ_P .

We start from the full covariance of the original system, which can be written in blocks as:

$$\Sigma = \begin{pmatrix} \Sigma_{XX} & \Sigma_{XY} \\ \Sigma_{YX} & \Sigma_{YY} \end{pmatrix}, \quad (\text{A2})$$

where $\Sigma_{XY} = \Sigma_{YX}^\top$. Without loss of generality, we assume that all X_i and Y_j are zero-mean and unit-variance, such that all diagonal elements of Σ_{XX} and Σ_{YY} are 1. This is possible because mutual information is invariant under isomorphisms in both arguments [87].

Instead of working directly on the correlation matrices, we consider their Cholesky decomposition. Every lower-triangular matrix M with positive diagonal uniquely determines a symmetric positive definite matrix S through the bijective mapping:

$$M \rightarrow S : S = MM^\top \quad (\text{A3a})$$

$$S \rightarrow M : M = \text{chol}(S), \quad (\text{A3b})$$

where $\text{chol}(S)$ is the Cholesky decomposition of S .

Hence, let $L = \text{chol}(\Sigma)$ be the Cholesky decomposition of the full system (i.e. $\Sigma = LL^\top$). We can write this in blocks:

$$\Sigma = LL^\top = \begin{pmatrix} L_{XX} & 0 \\ L_{YX} & L_{YY} \end{pmatrix} \begin{pmatrix} L_{XX}^\top & L_{YX}^\top \\ 0 & L_{YY}^\top \end{pmatrix} = \begin{pmatrix} L_{XX}L_{XX}^\top & L_{XX}L_{YX}^\top \\ L_{YX}L_{XX}^\top & L_{YX}L_{YX}^\top + L_{YY}L_{YY}^\top \end{pmatrix}, \quad (\text{A4})$$

where L_{XX} and L_{YY} are lower-triangular diagonal-positive matrices, and L_{YX} is any real matrix with entries $\in [-1, 1]$. A similar structure holds for Σ^Q .

To incorporate the constraints of Δ_P , we explicitly enforce that all the cross-covariances between the X_i 's and the Y_j 's are equal to those in the original system, i.e.

$$\Sigma_{YX}^Q = \Sigma_{YX}. \quad (\text{A5})$$

Thus, comparing the off-diagonal terms of Eqs. (A2)-(A4) and imposing Eq.(A5), we obtain:

$$\Sigma_{YX}^Q = L_{YX}^Q L_{XX}^{Q,\top} = \Sigma_{YX} \implies L_{YX}^Q = \Sigma_{YX} \left(L_{XX}^{Q,\top} \right)^{-1}. \quad (\text{A6})$$

This suggests that any Cholesky matrix L^Q of a distribution $Q \in \Delta_P$ must have the following block structure:

$$L^Q = \begin{pmatrix} L_{XX}^Q & 0 \\ \Sigma_{YX} (L_{XX}^Q)^\top{}^{-1} & L_{YY}^Q \end{pmatrix}. \quad (\text{A7})$$

There is one more constraint we need to satisfy: the fact that the diagonal of Σ^Q must be equal to 1. We achieve this by employing parametrisation techniques from the Parametrization Cookbook (PC) [53].

We begin with \mathbf{X} . Since the covariance of \mathbf{X} is simply $\Sigma_{XX}^Q = L_{XX} L_{XX}^\top$, we can make sure this constraint is satisfied by parametrising the space of correlation matrices in \mathbf{X} [53, Sec. 2.4.5].

Regarding \mathbf{Y} , its covariance is $\Sigma_{YY}^Q = L_{YX}^Q L_{YX}^{Q,\top} + L_{YY}^Q L_{YY}^{Q,\top}$. Since L_{XY}^Q is determined by L_{XX}^Q and Σ_{YX} , we want to parametrise L_{YY}^Q such that the diagonal of this sum is 1. Let $\mathbf{d} = \text{diag}(L_{YX}^Q L_{YX}^{Q,\top})$ be the vector of diagonal elements of the first summand above. As per PC, if M is a lower-triangular matrix and $S = MM^\top$, for S_{ii} to be equal to a , the i -th row of M must be a point in the half-sphere of radius \sqrt{a} . By inspecting the expression for Σ_{YY}^Q above, we conclude that L_{YY}^Q can be parametrised as a lower-triangular matrix where the i -th row is a point in the half-sphere of radius $\sqrt{1 - d_{i-1}}$.

Hence, this enables us to parametrise the optimisation set Δ_P by a correlation Cholesky factor, L_{XX}^Q , and a Cholesky factor with fixed diagonal, L_{YY}^Q . In turn, these can be easily mapped to a vector of real numbers [53].

In conclusion, starting from a point in a high-dimensional real space, we map the real numbers to L_{XX}^Q and L_{YY}^Q , calculate L^Q and thus Σ^Q , and finally compute $I_Q(\mathbf{X}; \mathbf{Y})$. Since all these maps are differentiable, we can perform the optimisation using standard gradient-based approaches.

Appendix B: Derivations and properties of \mathcal{W} - and \mathcal{M} -information

In this section, we first prove the formal link between \mathcal{W} - and \mathcal{M} -information and their formulation presented in Sec. (II B). Then, we discuss some properties of the probability distribution set Δ_P , and show that the mutual information $I(\mathbf{X}; \mathbf{Y})$ is a convex function of the marginal covariances.

In the following paragraphs, we assume \mathbf{X}, \mathbf{Y} to be Gaussian-distributed random variables with mean zero and correlation matrices Σ_{XX}, Σ_{YY} , respectively.

1. Definition of \mathcal{W} - and \mathcal{M} -information

In Sec. II B, we introduced \mathcal{W} - and \mathcal{M} -information as measures of low- and high-order interdependences, and then provided their functional form in Proposition 1 under Assumptions 1-3. In this paragraph, we present the rigorous proof of the Proposition.

For completeness, we first recall Assumptions 1-3:

Assumption 1 (*Pairwise dependence*). $\mathcal{W}(\mathbf{X}; \mathbf{Y})$ should only depend on the pairwise marginal distributions $P(X_i, Y_j)$.

Assumption 2 (*Non-negativity*). $\mathcal{W}(\mathbf{X}; \mathbf{Y}) \geq 0$ and $\mathcal{M}(\mathbf{X}; \mathbf{Y}) \geq 0$.

Assumption 3 (*Existence*). For any $P \in \Delta$, there exists a Q^* that has pairwise distributions $Q(X_i, Y_j) = P(X_i, Y_j)$ and no high-order information, i.e. it has the same \mathcal{W} of P while satisfying $\mathcal{M} = 0$.

We then have the following result:

Proposition 1. *Under Assumptions 1-3, the \mathcal{W} - and \mathcal{M} -information between two random vectors \mathbf{X} and \mathbf{Y} assume a unique functional form given by*

$$\mathcal{W}(\mathbf{X}; \mathbf{Y}) = \min_{Q \in \Delta_P} I_Q(\mathbf{X}; \mathbf{Y}), \quad (3)$$

$$\mathcal{M}(\mathbf{X}; \mathbf{Y}) = I(\mathbf{X}; \mathbf{Y}) - \mathcal{W}(\mathbf{X}; \mathbf{Y}), \quad (4)$$

with $\Delta_P := \{Q \in \Delta : Q(X_i, Y_j) = P(X_i, Y_j) \forall i, j\}$.

Proof. Let's denote with \mathcal{W} and \mathcal{M} the low- and high-order dependencies, respectively. We want to decompose the joint mutual information between \mathbf{X} and \mathbf{Y} such that:

$$I(\mathbf{X}; \mathbf{Y}) = \mathcal{W}(\mathbf{X}; \mathbf{Y}) + \mathcal{M}(\mathbf{X}; \mathbf{Y}). \quad (\text{B1})$$

Let's now consider a generic distribution $Q \in \Delta_P$. Analogously to Eq. (B1), its mutual information reads

$$\begin{aligned} I_Q(\mathbf{X}; \mathbf{Y}) &= \mathcal{W}_Q(\mathbf{X}; \mathbf{Y}) + \mathcal{M}_Q(\mathbf{X}; \mathbf{Y}) \\ &= \mathcal{W}(\mathbf{X}; \mathbf{Y}) + \mathcal{M}_Q(\mathbf{X}; \mathbf{Y}), \end{aligned} \quad (\text{B2})$$

where the second step follows from the fact that \mathcal{W}_Q only depends on the pairwise marginal distributions, and is therefore constant in Δ_P (Assumption 1). By minimising the LHS and RHS of Eq.(B2), we obtain

$$\begin{aligned} \min_{Q \in \Delta_P} I_Q(\mathbf{X}; \mathbf{Y}) &= \min_{Q \in \Delta_P} (\mathcal{W}_Q(\mathbf{X}; \mathbf{Y}) + \mathcal{M}_Q(\mathbf{X}; \mathbf{Y})) \\ &= \mathcal{W}(\mathbf{X}; \mathbf{Y}) + \min_{Q \in \Delta_P} \mathcal{M}_Q(\mathbf{X}; \mathbf{Y}) \\ &= \mathcal{W}(\mathbf{X}; \mathbf{Y}), \end{aligned} \quad (\text{B3})$$

where the last step follows from Assumptions 2-3, which ensure that $\exists Q^* \in \Delta_P$ s.t. $\min_{Q \in \Delta_P} \mathcal{M}_Q(\mathbf{X}; \mathbf{Y}) = \mathcal{M}_{Q^*}(\mathbf{X}; \mathbf{Y}) = 0$. This concludes the first statement of the Proposition.

The second part then directly follows from Eq.(B1):

$$\mathcal{M}(\mathbf{X}; \mathbf{Y}) = I(\mathbf{X}; \mathbf{Y}) - \mathcal{W}(\mathbf{X}; \mathbf{Y}). \quad (\text{B4})$$

□

2. Domain Δ_P

Let's now focus on the optimisation set Δ_P . We have the following result:

Proposition 4 (Convexity of Δ_P). *For \mathbf{X}, \mathbf{Y} Gaussian random variables, the probability distribution domain*

$$\Delta_P := \{Q \in \Delta : Q(X_i, Y_j) = P(X_i, Y_j) \forall i, j\} \quad (\text{B5})$$

is a convex set.

Proof. The space Δ of all probability distributions of \mathbf{X}, \mathbf{Y} corresponds to the space of all correlation matrices, which defines a region in the parameter space called elliptope – a convex subset of Euclidean space bounded by elliptical surfaces. Since the optimisation domain Δ_P is obtained by fixing the pairwise marginal distributions within Δ (Eq. (B5)), this consists in a slicing operation, which maintains the convexity property of the subset Δ_P . □

As explained in Appendix A, we then can parametrise the correlation matrices in Δ_P by using Eq. (A7), which imposes the constraints on the marginal distributions for any valid Cholesky factors L_{XX} and L_{YY} . However, for computational purposes, there is one additional requirement to satisfy. Since we want Σ_{YY} to be a correlation matrix, Eq. (A4) implies $\text{diag}(L_{YX}L_{YX}^\top + L_{YY}L_{YY}^\top) = 1$, which entails an extra constraint on the parameters of L_{XX} :

Lemma 1 (Optimisation constraint). *For any $Q \in \Delta_P$, the Cholesky factor L_{XX}^Q of Eq. (A7) needs to satisfy*

$$\text{diag}(L_{YX}L_{YX}^\top) = \text{diag}(\Sigma_{YX}\Sigma_{XX}^{Q,-1}\Sigma_{YX}^\top) < 1, \quad (\text{B6})$$

where $\Sigma_{XX}^Q = L_{XX}^Q L_{XX}^{Q,\top}$.

Although in theory Lemma 1 constrains our optimisation procedure by imposing an additional condition on L_{XX}^Q , we see that in practice this is naturally resolved by the properties we prove below.

3. Convexity of $I(\mathbf{X}; \mathbf{Y})$

We now turn to the properties of the mutual information $I(\mathbf{X}; \mathbf{Y})$. For ease of notation, in the rest of this paragraph we denote with Σ_X and Σ_Y the correlation matrices of \mathbf{X}, \mathbf{Y} , with dimensions $d_X \times d_X$ and $d_Y \times d_Y$ respectively, and with A the cross-correlation term Σ_{XY} . Hence the full covariance matrix of the system reads

$$\Sigma = \begin{pmatrix} \Sigma_X & A \\ A^\top & \Sigma_Y \end{pmatrix}. \quad (\text{B7})$$

We start by writing explicitly the expression of the mutual information [88] for Gaussian variables:

$$\begin{aligned} I(\mathbf{X}; \mathbf{Y}) &= \frac{1}{2} \log \left(\frac{\det(\Sigma_X) \det(\Sigma_Y)}{\det(\Sigma)} \right) \\ &= \frac{1}{2} \log \left(\frac{\det(\Sigma_Y)}{\det(\Sigma_Y - A \Sigma_X^{-1} A^\top)} \right), \end{aligned} \quad (\text{B8})$$

where in the second step we made use of the Schur-complement property

$$\det(\Sigma) = \det(\Sigma_X) \det(\Sigma_Y - A \Sigma_X^{-1} A^\top). \quad (\text{B9})$$

Thus, the objective function of the optimisation is a real-valued function of positive definite matrices

$$\begin{aligned} f: S_{d_X}^{++} \times S_{d_Y}^{++} &\rightarrow \mathbb{R} \\ (\Sigma_X, \Sigma_Y) &\mapsto I(\mathbf{X}, \mathbf{Y}), \end{aligned} \quad (\text{B10})$$

where S_n^{++} is the space of positive definite $n \times n$ matrices.

In the following, we prove that f is convex. However, to reach the main Proposition, we first need some results on positive definite matrices.

Definition 1. *A symmetric matrix $A \in \mathbb{R}^{n \times n}$ is positive definite if, for all non-zero vectors $x \in \mathbb{R}^n$, the following holds:*

$$x^\top A x > 0. \quad (\text{B11})$$

Additionally, an ordering structure can be imposed on the space S_n^{++} :

Definition 2. *Let $A, B \in S_n^{++}$. We say that A is strictly smaller than B in the Loewner sense if their difference is positive definite, i.e.*

$$A \prec B \quad \text{if} \quad B - A \in S_n^{++}. \quad (\text{B12})$$

Using this partial ordering, we can indicate that A is a positive definite matrix by writing $A \succ 0$.

With these definitions at hand, we can continue in our derivation. We start by reminding of a standard result:

Lemma 2 (Square of positive definite matrix). *A matrix $A \in \mathbb{R}^{n \times n}$ is positive definite if and only if it has a unique positive definite square root $A^{1/2}$:*

$$A \in S_n^{++} \iff \exists! A^{1/2} \in S_n^{++} \text{ s.t. } A^{1/2} A^{1/2} = A. \quad (\text{B13})$$

Proof. See e.g. Refs. [89, 90]. □

Directly following from Lemma 2, we have a useful property:

Lemma 3. *Given $A, B \in S_n^{++}$, then $A^{1/2}BA^{1/2} \in S_n^{++}$.*

Proof. Consider the matrix $C = A^{1/2}BA^{1/2}$. We show that C is symmetric and positive definite. Since $A^{1/2}$ and B are symmetric (Lemma 2 and hypothesis), we have

$$C^\top = (A^{1/2}BA^{1/2})^\top = A^{1/2}B^\top A^{1/2} = A^{1/2}BA^{1/2} = C, \quad (\text{B14})$$

so C is symmetric.

Then, let $x \in \mathbb{R}^n$, $x \neq 0$, and define $y = A^{1/2}x$. Since $A^{1/2}$ is invertible, $y \neq 0$. Then,

$$x^\top Cx = x^\top A^{1/2}BA^{1/2}x = y^\top By > 0, \quad (\text{B15})$$

because $B \in S_n^{++}$. Hence, $C = A^{1/2}BA^{1/2} \in S_n^{++}$. \square

Although the product of positive definite matrices is not in general positive definite, interesting properties hold for the trace of products:

Lemma 4. *Given $A, B, C \in S_n^{++}$, we have*

$$\text{a) } \text{Tr}(AB) > 0 \quad (\text{B16})$$

$$\text{b) } \text{Tr}(ABAC) > 0. \quad (\text{B17})$$

Proof. a) We have

$$\begin{aligned} \text{Tr}(AB) &\stackrel{\text{(a)}}{=} \text{Tr}(A^{1/2}A^{1/2}B) \\ &\stackrel{\text{(b)}}{=} \text{Tr}(A^{1/2}BA^{1/2}) \\ &\stackrel{\text{(c)}}{>} 0, \end{aligned} \quad (\text{B18})$$

where in (a) we used Lemma 2, in (b) the cyclic property of the trace, and (c) follows from $A^{1/2}BA^{1/2}$ being positive definite (Lemma 3).

b) We can write

$$\begin{aligned} \text{Tr}(ABAC) &= \text{Tr}(A^{1/2}BA^{1/2}A^{1/2}CA^{1/2}) \\ &= \text{Tr}(\tilde{B}\tilde{C}) \\ &> 0, \end{aligned} \quad (\text{B19})$$

where we introduced the positive definite matrices $\tilde{B} \equiv A^{1/2}BA^{1/2}$ and $\tilde{C} \equiv A^{1/2}CA^{1/2}$, and used part a) and Lemma 3. \square

Finally, we provide a result on the monotonicity of the trace operator:

Lemma 5. *Consider $A, B \in S_n^{++}$ so that $A \succ B$. Then $\text{Tr}(A^2) > \text{Tr}(B^2)$.*

Proof. Let $C \equiv A - B$. By definition of $A \succ B$, we have that $C \in S_n^{++}$. We can then write

$$\begin{aligned} \text{Tr}(A^2) - \text{Tr}(B^2) &= \text{Tr}((B + C)^2) - \text{Tr}(B^2) \\ &\stackrel{\text{(a)}}{=} 2\text{Tr}(BC) + \text{Tr}(C^2) \\ &\stackrel{\text{(b)}}{>} 0, \end{aligned} \quad (\text{B20})$$

where in (a) we expanded $A = B + C$ and used linearity of the trace operator, and (b) follows from positive definiteness of B, C (Lemma 4). \square

We are now ready to state the main result:

Proposition 2. *Given \mathbf{X}, \mathbf{Y} multivariate jointly Gaussian random variables with non-singular marginal and cross-covariances, their \mathcal{W} -information is a convex function in the marginal covariances of \mathbf{X}, \mathbf{Y} .*

Proof. Since f is convex if and only if it is convex along any direction in its domain, it is sufficient to show convexity along any line. Using a real parameter t , we parametrise such a generic line as

$$\Sigma_X = X_0 + tX, \quad \Sigma_Y = Y_0 + tY, \quad (\text{B21})$$

where $X_0, X, \in S_{d_X}^{++}$ and $Y_0, Y \in S_{d_Y}^{++}$, with $d_X \times d_X$ and $d_Y \times d_Y$ the dimensions of Σ_X and Σ_Y , respectively. Therefore, we define $g(t) := f(X_0 + tX, Y_0 + tY) \forall t > 0$ s.t. $X_0 + tX \succ 0$ and $Y_0 + tY \succ 0$. Using this manipulation, we are now dealing with a real-valued function of a real variable:

$$\begin{aligned} g: \mathbb{R} &\rightarrow \mathbb{R} \\ t &\mapsto I(\mathbf{X}, \mathbf{Y}). \end{aligned} \quad (\text{B22})$$

Using Eq. (B8), we can write g explicitly as

$$g(t) = \log(\det(\Sigma_Y)) - \log(\det(\Sigma_Y - A\Sigma_X^{-1}A^\top)), \quad (\text{B23})$$

where Σ_X and Σ_Y should be interpreted as functions of t as per Eq. (B21).

Following [51, 52], we prove strict convexity by showing that the second derivative $d^2g(t)/dt^2$ is positive $\forall t > 0$.

First Derivative:

$$\frac{dg(t)}{dt} = \text{Tr}(\Sigma_Y^{-1}Y) - \text{Tr}((\Sigma_Y - A\Sigma_X^{-1}A^\top)^{-1}(Y + A\Sigma_X^{-1}X\Sigma_X^{-1}A^\top)), \quad (\text{B24})$$

where we used the identities [91]:

$$\frac{d(\log(\det(X)))}{d\alpha} = \text{Tr}\left(X^{-1}\frac{dX}{d\alpha}\right), \quad (\text{B25})$$

$$\frac{dX^{-1}}{d\alpha} = -X^{-1}\frac{dX}{d\alpha}X^{-1}. \quad (\text{B26})$$

Second Derivative:

$$\begin{aligned} \frac{d^2g(t)}{dt^2} &= -\text{Tr}(\Sigma_Y^{-1}Y\Sigma_Y^{-1}Y) + \\ &\quad + \text{Tr}((\Sigma_Y - A\Sigma_X^{-1}A^\top)^{-1}(Y + A\Sigma_X^{-1}X\Sigma_X^{-1}A^\top)(\Sigma_Y - A\Sigma_X^{-1}A^\top)^{-1}(Y + A\Sigma_X^{-1}X\Sigma_X^{-1}A^\top)) + \\ &\quad + 2\text{Tr}((\Sigma_Y - A\Sigma_X^{-1}A^\top)^{-1}(A\Sigma_X^{-1}X\Sigma_X^{-1}X\Sigma_X^{-1}A^\top)) \\ &\stackrel{(a)}{=} -\text{Tr}(\Sigma_Y^{-1}Y\Sigma_Y^{-1}Y) + \text{Tr}((\Sigma_Y - A\Sigma_X^{-1}A^\top)^{-1}Y(\Sigma_Y - A\Sigma_X^{-1}A^\top)^{-1}Y)) + \\ &\quad + 2\text{Tr}((\Sigma_Y - A\Sigma_X^{-1}A^\top)^{-1}Y(\Sigma_Y - A\Sigma_X^{-1}A^\top)^{-1}(A\Sigma_X^{-1}X\Sigma_X^{-1}A^\top)) + \\ &\quad + \text{Tr}((\Sigma_Y - A\Sigma_X^{-1}A^\top)^{-1}(A\Sigma_X^{-1}X\Sigma_X^{-1}A^\top)(\Sigma_Y - A\Sigma_X^{-1}A^\top)^{-1}(A\Sigma_X^{-1}X\Sigma_X^{-1}A^\top)) + \\ &\quad + 2\text{Tr}((\Sigma_Y - A\Sigma_X^{-1}A^\top)^{-1}(A\Sigma_X^{-1}X\Sigma_X^{-1}X\Sigma_X^{-1}A^\top)) \\ &\stackrel{(b)}{>} 2\text{Tr}((\Sigma_Y - A\Sigma_X^{-1}A^\top)^{-1}Y(\Sigma_Y - A\Sigma_X^{-1}A^\top)^{-1}(A\Sigma_X^{-1}X\Sigma_X^{-1}A^\top)) + \\ &\quad + \text{Tr}((\Sigma_Y - A\Sigma_X^{-1}A^\top)^{-1}(A\Sigma_X^{-1}X\Sigma_X^{-1}A^\top)(\Sigma_Y - A\Sigma_X^{-1}A^\top)^{-1}(A\Sigma_X^{-1}X\Sigma_X^{-1}A^\top)) + \\ &\quad + 2\text{Tr}((\Sigma_Y - A\Sigma_X^{-1}A^\top)^{-1}(A\Sigma_X^{-1}X\Sigma_X^{-1}X\Sigma_X^{-1}A^\top)) \\ &\stackrel{(c)}{>} 0. \end{aligned} \quad (\text{B27})$$

In (a) we expanded the second expression and used the cyclic property of the trace to sum two equal terms, whereas in (b) we noticed that

$$\text{Tr}((\Sigma_Y - A\Sigma_X^{-1}A^\top)^{-1}Y(\Sigma_Y - A\Sigma_X^{-1}A^\top)^{-1}Y) > \text{Tr}(\Sigma_Y^{-1}Y\Sigma_Y^{-1}Y). \quad (\text{B28})$$

To see this, let's introduce the shorthand $S \equiv (\Sigma_Y - A\Sigma_X^{-1}A^\top)$, i.e. S is the Schur-complement of Σ w.r.t. to Σ_X . Since Σ is positive definite and Σ_X is invertible, it follows that S is also positive definite [92]. We can therefore rewrite the traces of Eq. (B28) as

$$\text{Tr}(S^{-1}YQ^{-1}Y) = \text{Tr}(Y^{1/2}S^{-1}Y^{1/2}Y^{1/2}S^{-1}Y^{1/2}) \equiv \text{Tr}(M^2) \quad (\text{B29})$$

$$\text{Tr}(\Sigma_Y^{-1}Y\Sigma_Y^{-1}Y) = \text{Tr}(Y^{1/2}\Sigma_Y^{-1}Y^{1/2}Y^{1/2}\Sigma_Y^{-1}Y^{1/2}) \equiv \text{Tr}(N^2), \quad (\text{B30})$$

where $M \equiv Y^{1/2}S^{-1}Y^{1/2}$ and $N \equiv Y^{1/2}\Sigma_Y^{-1}Y^{1/2}$ are now positive definite matrices (Lemma 3). Moreover, we have that $M \succ N$:

$$\begin{aligned} A\Sigma_X^{-1}A^\top \succ 0 &\implies \Sigma_Y - A\Sigma_X^{-1}A^\top \prec \Sigma_Y & (\text{B31}) \\ &\implies (\Sigma_Y - A\Sigma_X^{-1}A^\top)^{-1} \succ \Sigma_Y^{-1} \\ &\implies Y^{1/2}(\Sigma_Y - A\Sigma_X^{-1}A^\top)^{-1}Y^{1/2} \succ Y^{1/2}\Sigma_Y^{-1}Y^{1/2} \\ &\equiv M \succ N, \end{aligned}$$

where the third implication holds as $Y^{1/2}$ is positive definite. Therefore, having Eqs. (B29)-(B30)-(B31), we can apply Lemma 5 and obtain Eq. (B28).

Finally, in the last step (c) we made use of Lemma 4.

Thus, we proved that the mutual information is convex along a generic line in the domain Δ_P , and therefore that it is globally convex. \square

The proof presented here assumes that Σ_X, Σ_Y, A are well-defined full-rank matrices, i.e. $\Sigma_X \in \mathbb{R}^{d_X \times d_X}$, $\Sigma_Y \in \mathbb{R}^{d_Y \times d_Y}$, and $A \in \mathbb{R}^{d_Y \times d_X}$ and $\text{rank}(\Sigma_X) = d_X$, $\text{rank}(\Sigma_Y) = d_Y$, $\text{rank}(A) = \min(d_X, d_Y)$. In case these conditions are not met, then the mutual information is not convex. As a counterexample, consider $A_{ij} = 0 \forall i, j$, then $I(\mathbf{X}; \mathbf{Y}) = 0 \forall \Sigma_X, \Sigma_Y \in S_n^{++}$, with $n = d_X = d_Y$.

4. Boundaries of Δ_P

Although the minimisation problem is well-posed, we need to make sure that the optimisation procedure does not step outside the boundaries of Δ_P , where the function is not defined (Lemma 1). Luckily, it is easy to prove that on the boundary of the domain Δ_P , the mutual information becomes infinite, which is our second main result:

Proposition 3. *Given \mathbf{X}, \mathbf{Y} multivariate jointly Gaussian random variables with non-singular marginal covariances, the probability distribution Q^* that minimises Eq. (3) is an inner point of Δ_P .*

Proof. In the parametrisation given by Eq.(A4), the border of Δ_P is characterised by $\text{diag}(L_{YX}L_{YX}^\top)_i = 1$ for some $i = 1, \dots, n$. If one such diagonal entry is 1, it follows that $\text{diag}(L_{YX}L_{YX}^\top)_i = 0$ and $\text{diag}(L_{YY})_i = 0$, which implies $\det(\Sigma) = \det(L)^2 = 0$. On the other hand, $\det(\Sigma_{XX}) > 0$ and $\det(\Sigma_{YY}) > 0$ by hypotheses, hence on the boundary we obtain

$$I(\mathbf{X}; \mathbf{Y}) = \frac{1}{2} \log \left(\frac{\det(\Sigma_X) \det(\Sigma_Y)}{\det(\Sigma)} \right) \rightarrow +\infty. \quad (\text{B32})$$

Thus, the distribution Q^* has to be an inner point of Δ_P

\square

Note that with the parametrisation chosen, the hypotheses of Proposition 3 can be further relaxed, as we only need L_{XX} and L_{YY} to be non-singular upper diagonal matrices. In fact, $\det(L_{XX}) > 0 \implies \det(\Sigma_{XX}) > 0$, and

$$\begin{aligned} \det(\Sigma_{YY}) &= \det(L_{YX}L_{YX}^\top + L_{YY}L_{YY}^\top) \\ &\stackrel{(a)}{\geq} \det(L_{YX}L_{YX}^\top) + \det(L_{YY}L_{YY}^\top) \\ &\stackrel{(b)}{=} \det(L_{YX}L_{YX}^\top) \\ &> 0, \end{aligned} \tag{B33}$$

where in (a) we used the matrix concavity of the map $A \mapsto \det(A)$, and in (b) the fact that $L_{YX}L_{YX}^\top$ and $L_{YY}L_{YY}^\top$ are positive definite. The result then follows in the same way from Eq. (B32).

This result also explains why we can avoid addressing the issue raised in Lemma 1. Since $I(\mathbf{X}; \mathbf{Y})$ is continuous at any inner point, its gradients must diverge approaching the boundaries. This ensures that standard optimisation techniques such as Stochastic Gradient Descent do not step outside the domain even without directly imposing the extra constraints.

Again, we remind that if A is not full-rank, then the minimum of the mutual information may lie on the boundary as $\det(L_{YX})$ could also vanish.

Appendix C: BROJA-ΦID

Here we outline the complete derivation of the BROJA-ΦID method presented in Sec. IV. We adopt a practical approach to the framework, focusing on the equations required to compute the ΦID terms. For rigorous derivations, theoretical details, and a more general treatment, we refer to the original work [35].

Given two bivariate random variables $\mathbf{X} = (X_1, X_2)$ and $\mathbf{Y} = (Y_1, Y_2)$, we aim to decompose the joint mutual information of the system $I(\mathbf{X}; \mathbf{Y})$ into redundant (R), unique (U), and synergistic components (S), both in \mathbf{X} and \mathbf{Y} . Following [35], we start by writing down the functional form of marginal and joint mutual information in terms of the ΦID atoms:

$$I(X_1; Y_1) = R \rightarrow R + R \rightarrow U_1 + U_1 \rightarrow R + U_1 \rightarrow U_1 \tag{C1}$$

$$I(X_2; Y_2) = R \rightarrow R + R \rightarrow U_2 + U_2 \rightarrow R + U_2 \rightarrow U_2 \tag{C2}$$

$$I(X_1; Y_2) = R \rightarrow R + R \rightarrow U_2 + U_1 \rightarrow R + U_1 \rightarrow U_2 \tag{C3}$$

$$I(X_2; Y_1) = R \rightarrow R + R \rightarrow U_1 + U_2 \rightarrow R + U_2 \rightarrow U_1 \tag{C4}$$

$$\begin{aligned} I(X_1, X_2; Y_1) &= R \rightarrow R + R \rightarrow U_1 + U_1 \rightarrow R + U_1 \rightarrow U_1 + \\ &U_2 \rightarrow R + U_2 \rightarrow U_1 + S \rightarrow R + S \rightarrow U_1 \end{aligned} \tag{C5}$$

$$\begin{aligned} I(X_1, X_2; Y_2) &= R \rightarrow R + R \rightarrow U_2 + U_1 \rightarrow R + U_1 \rightarrow U_2 + \\ &U_2 \rightarrow R + U_2 \rightarrow U_2 + S \rightarrow R + S \rightarrow U_2 \end{aligned} \tag{C6}$$

$$\begin{aligned} I(X_1; Y_1, Y_2) &= R \rightarrow R + U_1 \rightarrow R + R \rightarrow U_1 + U_1 \rightarrow U_1 + \\ &R \rightarrow U_2 + U_1 \rightarrow U_2 + R \rightarrow S + U_1 \rightarrow S \end{aligned} \tag{C7}$$

$$\begin{aligned} I(X_2; Y_1, Y_2) &= R \rightarrow R + U_2 \rightarrow R + R \rightarrow U_1 + U_2 \rightarrow U_1 + \\ &R \rightarrow U_2 + U_2 \rightarrow U_2 + R \rightarrow S + U_2 \rightarrow S \end{aligned} \tag{C8}$$

$$\begin{aligned} I(X_1, X_2; Y_1, Y_2) &= R \rightarrow R + U_1 \rightarrow R + U_2 \rightarrow R + S \rightarrow R + \\ &R \rightarrow U_1 + U_1 \rightarrow U_1 + U_2 \rightarrow U_1 + S \rightarrow U_1 + \\ &R \rightarrow U_2 + U_1 \rightarrow U_2 + U_2 \rightarrow U_2 + S \rightarrow U_2 + \\ &R \rightarrow S + U_1 \rightarrow S + U_2 \rightarrow S + S \rightarrow S. \end{aligned} \tag{C9}$$

Then, six additional constraints are given by six BROJA-PID decompositions on different parts of the system. Specifically, if, for instance, we consider X_1, X_2 as sources and Y_1 as target, we can perform a PID that

provides the redundancy $R(X_1, X_2; Y_1)$, which is equal to

$$R(X_1, X_2; Y_1) = R \rightarrow R + R \rightarrow U_1. \quad (\text{C10})$$

Performing a similar procedure on all possible combinations of sources and targets, we obtain the remaining 5 redundancies:

$$R(X_1, X_2; Y_1, Y_2) = R \rightarrow R + R \rightarrow U_1 + R \rightarrow U_2 + R \rightarrow S \quad (\text{C11})$$

$$R(X_1, X_2; Y_2) = R \rightarrow R + R \rightarrow U_2 \quad (\text{C12})$$

$$R(Y_1, Y_2; X_1, X_2) = R \rightarrow R + U_1 \rightarrow R + U_2 \rightarrow R + S \rightarrow R \quad (\text{C13})$$

$$R(Y_1, Y_2; X_1) = R \rightarrow R + U_1 \rightarrow R \quad (\text{C14})$$

$$R(Y_1, Y_2; X_2) = R \rightarrow R + U_2 \rightarrow R. \quad (\text{C15})$$

Finally, to uniquely determine all 16 atoms, we need an additional condition. We attain this by including all the low-order terms, i.e. those that depend only on redundancy and unique information, in the \mathcal{W} -information. We justify this step as follows:

1. redundancies and unique information depend only on the pairwise marginals;
2. therefore, all atoms that contain only redundancies and unique information are constant in Δ_P .
3. There is at least one distribution $Q^* \in \Delta_P$ which has only redundancies and unique information, with all other atoms being zero;
4. this is the distribution that the optimiser will find.
5. Hence, $\min_{Q \in \Delta_P} I_Q(\mathbf{X}; \mathbf{Y})$ equals the sum of all redundancies and unique information.

Thus, we can write

$$\begin{aligned} \mathcal{W} = & R \rightarrow R + R \rightarrow U_1 + R \rightarrow U_2 + \\ & U_1 \rightarrow R + U_1 \rightarrow U_1 + U_1 \rightarrow U_2 + \\ & U_2 \rightarrow R + U_2 \rightarrow U_1 + U_2 \rightarrow U_2. \end{aligned} \quad (\text{C16})$$

Following this reasoning, we can also express \mathcal{M} -information in terms of the remaining Φ ID atoms, obtaining:

$$\begin{aligned} \mathcal{M} = & R \rightarrow S + U_1 \rightarrow S + U_2 \rightarrow S + \\ & S \rightarrow R + S \rightarrow U_1 + S \rightarrow U_2 + \\ & S \rightarrow S. \end{aligned} \quad (\text{C17})$$

In other words, \mathcal{M} -information contains all the atoms that involve synergistic terms, either in \mathbf{X} or \mathbf{Y} .

Thus, the Φ ID atoms can be computed by solving the linear system of equations given by Eqs. (C1)-(C16).

Appendix D: Methods and data

1. Toy models

Here we give the details of the toy models presented in Secs. III A-IV.

Considering two univariate time series X_t and Y_t that follow Gaussian dynamics, we focus on the Φ ID decomposition of the mutual information $I(X_t, Y_t; X_{t+1}, Y_{t+1})$. To validate our methods in controlled scenarios, we construct 16 systems, each designed to maximally express one of the atoms in the decomposition. Defining an auxiliary Gaussian variable $Z_t \sim \mathcal{N}(0, 1)$ and a Gaussian noise term $\varepsilon_t \sim \mathcal{N}(0, 10^{-4})$, we repeatedly sample these terms to obtain a time series, and then generate each of the 16 systems as follows, with the dominant atom indicated alongside each configuration:

1. $R \rightarrow R$: we correlate both the sources and the targets together:

$$X_t = Z_t + \varepsilon \quad (\text{D1a})$$

$$Y_t = Z_t + \varepsilon \quad (\text{D1b})$$

$$X_{t+1} = Z_t + \varepsilon \quad (\text{D1c})$$

$$Y_{t+1} = Z_t + \varepsilon; \quad (\text{D1d})$$

2. $R \rightarrow U_1$: we correlate the sources with the first target:

$$X_t = Z_t + \varepsilon \quad (\text{D2a})$$

$$Y_t = Z_t + \varepsilon \quad (\text{D2b})$$

$$X_{t+1} = Z_t + \varepsilon \quad (\text{D2c})$$

$$Y_{t+1} = \varepsilon; \quad (\text{D2d})$$

3. $R \rightarrow U_2$: we correlate the sources with the second target:

$$X_t = Z_t + \varepsilon \quad (\text{D3a})$$

$$Y_t = Z_t + \varepsilon \quad (\text{D3b})$$

$$X_{t+1} = \varepsilon \quad (\text{D3c})$$

$$Y_{t+1} = Z_t + \varepsilon; \quad (\text{D3d})$$

4. $R \rightarrow S$: we correlate the targets and make both sources functions of the sum of the targets:

$$X_{t+1} = 100\varepsilon \quad (\text{D4a})$$

$$Y_{t+1} = 100\varepsilon \quad (\text{D4b})$$

$$X_t = X_{t+1} + Y_{t+1} + \varepsilon \quad (\text{D4c})$$

$$Y_t = X_{t+1} + Y_{t+1} + \varepsilon; \quad (\text{D4d})$$

5. $U_1 \rightarrow R$: we correlate the first source with the targets:

$$X_t = Z_t + \varepsilon \quad (\text{D5a})$$

$$Y_t = \varepsilon \quad (\text{D5b})$$

$$X_{t+1} = Z_t + \varepsilon \quad (\text{D5c})$$

$$Y_{t+1} = Z_t + \varepsilon; \quad (\text{D5d})$$

6. $U_1 \rightarrow U_1$: we correlate the first source with the first target:

$$X_t = Z_t + \varepsilon \quad (\text{D6a})$$

$$Y_t = \varepsilon \quad (\text{D6b})$$

$$X_{t+1} = Z_t + \varepsilon \quad (\text{D6c})$$

$$Y_{t+1} = \varepsilon; \quad (\text{D6d})$$

7. $U_1 \rightarrow U_2$: we correlate the first source with the second target:

$$X_t = Z_t + \varepsilon \quad (\text{D7a})$$

$$Y_t = \varepsilon \quad (\text{D7b})$$

$$X_{t+1} = \varepsilon \quad (\text{D7c})$$

$$Y_{t+1} = Z_t + \varepsilon; \quad (\text{D7d})$$

8. $U_1 \rightarrow S$: we correlate the targets and make the first source function of the sum of the targets:

$$X_{t+1} = Z_t + \varepsilon \quad (\text{D8a})$$

$$Y_{t+1} = Z_t + \varepsilon \quad (\text{D8b})$$

$$X_t = X_{t+1} + Y_{t+1} + \varepsilon \quad (\text{D8c})$$

$$Y_t = \varepsilon; \quad (\text{D8d})$$

9. $U_2 \rightarrow R$: we correlate the second source with both targets:

$$X_t = \varepsilon \quad (\text{D9a})$$

$$Y_t = Z_t + \varepsilon \quad (\text{D9b})$$

$$X_{t+1} = Z_t + \varepsilon \quad (\text{D9c})$$

$$Y_{t+1} = Z_t + \varepsilon; \quad (\text{D9d})$$

10. $U_2 \rightarrow U_1$: we correlate the second source with the first target:

$$X_t = \varepsilon \quad (\text{D10a})$$

$$Y_t = Z_t + \varepsilon \quad (\text{D10b})$$

$$X_{t+1} = Z_t + \varepsilon \quad (\text{D10c})$$

$$Y_{t+1} = \varepsilon; \quad (\text{D10d})$$

11. $U_2 \rightarrow U_2$: we correlate the second source with the second target:

$$X_t = \varepsilon \quad (\text{D11a})$$

$$Y_t = Z_t + \varepsilon \quad (\text{D11b})$$

$$X_{t+1} = \varepsilon \quad (\text{D11c})$$

$$Y_{t+1} = Z_t + \varepsilon; \quad (\text{D11d})$$

12. $U_2 \rightarrow S$: we correlate the targets and make the second source function of the sum of the targets:

$$X_{t+1} = 100\varepsilon \quad (\text{D12a})$$

$$Y_{t+1} = 100\varepsilon \quad (\text{D12b})$$

$$X_t = \varepsilon \quad (\text{D12c})$$

$$Y_t = X_{t+1} + Y_{t+1} + \varepsilon; \quad (\text{D12d})$$

13. $S \rightarrow R$: we correlate the sources and make both targets functions of the sum of the sources:

$$X_t = 100\varepsilon \quad (\text{D13a})$$

$$Y_t = 100\varepsilon \quad (\text{D13b})$$

$$X_{t+1} = X_t + Y_t + \varepsilon \quad (\text{D13c})$$

$$Y_{t+1} = X_t + Y_t + \varepsilon; \quad (\text{D13d})$$

14. $S \rightarrow U_1$: we correlate the sources and make the first target function of the sum of the sources:

$$X_t = 100\varepsilon \quad (\text{D14a})$$

$$Y_t = 100\varepsilon \quad (\text{D14b})$$

$$X_{t+1} = X_t + Y_t + \varepsilon \quad (\text{D14c})$$

$$Y_{t+1} = \varepsilon; \quad (\text{D14d})$$

15. $S \rightarrow U_2$: we correlate the sources and make the second target function of the sum of the sources:

$$X_t = 100\varepsilon \quad (\text{D15a})$$

$$Y_t = 100\varepsilon \quad (\text{D15b})$$

$$X_{t+1} = \varepsilon \quad (\text{D15c})$$

$$Y_{t+1} = X_t + Y_t + \varepsilon; \quad (\text{D15d})$$

16. $S \rightarrow S$: we correlate the sources and one target and make the other target function of the both sources and target:

$$X_t = 100\varepsilon \quad (\text{D16a})$$

$$Y_t = 100\varepsilon \quad (\text{D16b})$$

$$X_{t+1} = 100\varepsilon \quad (\text{D16c})$$

$$Y_{t+1} = X_t + Y_t - X_{t+1}\varepsilon. \quad (\text{D16d})$$

These systems provide the expected predominant atoms also with other definitions of Φ ID (e.g. the Minimal Mutual Information formulation introduced in Ref. [48] for PID, and generalised to Φ ID in Ref. [35]). Hence, we use them to test both the behaviour of $\mathcal{M}(X_t, Y_t; X_{t+1}, Y_{t+1})$, $\mathcal{W}(X_t, Y_t; X_{t+1}, Y_{t+1})$ (Sec. III A), and BROJA- Φ ID (Sec. IV).

2. VAR models

Vector Autoregression (VAR) is a statistical framework often used in statistics and complexity science to model the evolution of a dynamical system. VAR models have been applied in a variety of areas, such as sociology [93], economics [94], statistics [95], and beyond.

The advantage of employing VAR models lies in their capability to capture interdependencies in time series data [96], providing an efficient yet robust methodology to infer the system's information dynamics.

Specifically, given a multivariate time series $\mathbf{X}_t = (X_t^1, \dots, X_t^n)$, the defining VAR equation can be written as

$$\mathbf{X}_t = \sum_{l=1}^p A_l \mathbf{X}_{t-l} + \boldsymbol{\varepsilon}_t, \quad (\text{D17})$$

where A_l is the $n \times n$ matrix of coefficients for the timepoint $t - l$, $\boldsymbol{\varepsilon}$ a Gaussian noise term sampled from $\mathcal{N}(0, \mathbf{V})$, and p the VAR model order. Since this system captures contributions up to p timesteps in the past, the model is named VAR(p).

Once the parameters A and \mathbf{V} are fitted to the data, e.g. with standard techniques such as Ordinary Least Squares [97], one can use the Yule-Walker equations to estimate the autocovariance matrices of the system [98, 99], and thus construct the full covariance matrix.

Since the VAR models considered here are Gaussian stationary processes, we can then calculate \mathcal{W} - and \mathcal{M} -information as presented in Sec. II C. For simplicity, all the autoregressive systems considered in this paper are VAR(1) models.

3. Wilson-Cowan model

The Wilson–Cowan (WC) model is a foundational mathematical framework for describing the dynamics of interacting populations of excitatory and inhibitory neurons [100, 101]. Due to its generality and ease of applicability, the model has become one of the cornerstones of theoretical neuroscience and computational biology [102–106], setting the ground for various generalisations [107, 108].

Rather than tracking individual spikes, WC describes the average activity of large populations of excitatory and inhibitory neurons. This coarse-grained approach significantly reduces computational load while retaining enough dynamical richness to reproduce key neural phenomena such as oscillations, bistability, and critical transitions [109, 110].

The basic Wilson–Cowan equations are a pair of coupled non-linear ordinary differential equations (ODEs) that describe how the mean firing rates $E(t)$ and $I(t)$ evolve over time:

$$\tau_E \frac{dE(t)}{dt} = -E(t) + S_E(W_{EE}E(t) - W_{EI}I(t) + P_E(t) + \eta_E(t)), \quad (\text{D18})$$

$$\tau_I \frac{dI(t)}{dt} = -I(t) + S_I(W_{IE}E(t) - W_{II}I(t) + P_I(t) + \eta_I(t)), \quad (\text{D19})$$

where $E(t)$ and $I(t)$ are the mean firing rates of excitatory and inhibitory populations, τ_E and τ_I are their respective time constants, W_{XY} denotes the connection strength from population Y to X , $P_E(t)$ and $P_I(t)$ represent external inputs, $(\eta_E, \eta_I)^\top \sim \mathcal{N}(0, V)$ are Gaussian noise terms, and $S_E(\cdot)$ and $S_I(\cdot)$ are sigmoidal activation functions of the form:

$$S_X(x) = \frac{1}{1 + e^{-\alpha(x - \theta_X)}}, \quad (\text{D20})$$

where α controls the gain of the function, and θ_X the activation threshold for the species X .

For our simulations, the following standard parameters were employed:

- $\tau_E = \tau_I = 1.0$
- $P_E = P_I = 0.125$
- $W_{EE} = 10.0, W_{II} = 3.0$
- $\theta_E = 0.2, \theta_i = 4.0$
- $\alpha = 1.0$.

The coupling strengths W_{EI}, W_{IE} were varied across simulations, along with the noise correlation parameter in V :

$$V = \begin{pmatrix} 1 & c \\ c & 1 \end{pmatrix}. \quad (\text{D21})$$

After simulating the Wilson–Cowan model across a range of parameters, we fitted a Gaussian copula to the joint distribution of excitatory and inhibitory firing rates to estimate the system’s full covariance structure. While the underlying dynamics are non-linear and thus deviate from the Gaussianity assumption, prior work in information theory has demonstrated that Gaussian copulas can effectively capture statistical dependencies in such systems [111]. This is enabled by the invariance of mutual information under smooth invertible transformations, which allows copula-based approaches to retain sensitivity to non-linear interactions. Finally, \mathcal{W} - and \mathcal{M} -information were calculated on the system across time by following the algorithm of Sec. II C.

4. Neuropixel LFP data

We used local field potential (LFP) recordings from the publicly available dataset published by Steinmetz et al. (2019) [57], which includes high-density neural recordings across the mouse brain during a visually guided decision-making task. The dataset was collected using Neuropixels probes inserted into the left hemisphere of head-fixed mice performing a two-alternative unforced choice (2AUC) task. Recordings were made across 39 behavioural sessions from 10 mice, comprising a total of 92 probe insertions.

Each session includes simultaneous recordings from hundreds of neurons and LFP signals across multiple cortical and subcortical regions. A typical probe insertion spanned several anatomically and functionally distinct areas, enabling large-scale, distributed recordings. Task trials involved visual stimuli presented unilaterally, bilaterally, or not at all, with reward contingencies linked to the contrast and location of the stimulus. Mice responded by turning a wheel to indicate the side with higher contrast, or by withholding movement if no stimulus was present. Trials where equal-contrast bilateral stimuli were presented were rewarded randomly. This design allowed dissociation of neural signals related to sensory processing, motor action, and choice.

In addition to active task trials, the dataset includes passive viewing trials, conducted in the absence of task demands or reward. During these sessions, the same visual stimuli were presented while the animal remained disengaged, allowing comparison of evoked neural responses across different behavioural contexts.

Further details on surgical preparation, probe configuration, spike sorting, and behavioural training are described in the original study [57].

Appendix E: Additional results

In this paragraph we report further results on the synthetic systems, the bias and scalability analysis, and the Neuropixel mice brain data.

1. Bias and scalability study details

The analyses for the bias corrections and scalability were run on the High Performance Computing (HPC) cluster of Imperial College London, United Kingdom. In the case of the bias correction, we first sample 1000

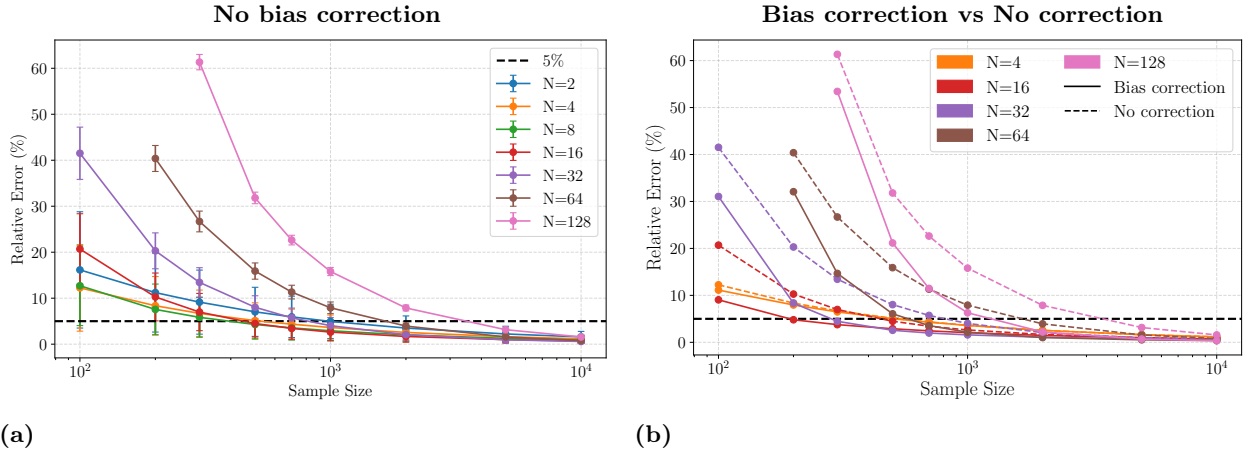


FIG. 5: (a) Bias estimation of \mathcal{W} -information against ground truth without bias correction for different system dimensions and sample sizes. Error bars represent the SEM. (b) Comparison of biases with and without bias correction. Error bars were removed for ease of visualisation.

covariance matrices from a Wishart distribution, we generate time series of different length by sampling from the original covariance, estimate the covariance from the data, and finally compute \mathcal{W} -information. We then repeat the process 100 times with different covariances and compute mean and Standard Error of the Mean (SEM) for each sample size (Fig. 2). For the scalability study, 1000 covariance matrices were randomly sampled from a Wishart distribution for each dimension, and then mean and SEM were estimated. In both cases, the optimisations were run as parallel jobs on the HPC, each requesting a maximum of 2 CPUs and 4 GB of memory.

To further analyse the effect of bias correction on the estimation of \mathcal{W} -information, we compare the bias corrected and non biased corrected results, noting that the correction significantly improves the convergence speed (Fig. 5).

2. High-dimensional autoregressive systems

Here we extend the analysis presented in Sec. III A to multivariate time series, studying the behaviour of \mathcal{M} -information on a larger modular autoregressive model. Focusing on $n = 10$ time series, we reproduce Experiment 3 by setting the evolution coefficients as

$$A = \begin{pmatrix} \mathcal{A} & \mathcal{B} \\ \mathcal{B} & \mathcal{A} \end{pmatrix}, \quad (\text{E1})$$

where \mathcal{A} is a matrix of size 5×5 with all entries equal to a , and \mathcal{B} is a 5×5 matrix with all entries equal to b , with $a, b \in (-1, 1)$. The residual covariance matrix V is equal to c on the off-diagonal, and ones on the diagonal, i.e. $V_{ij} = c$ for $i \neq j$ and $V_{ii} = 1$. As in Sec. III A, we simulate the dynamics of Eq. (7), rescaling the matrix A so that the system provides the same joint mutual information for each choice of (a, b) , and then calculate \mathcal{W} - and \mathcal{M} -information.

Similarly to the $n = 2$ case, we notice that for low values of noise \mathcal{M} -information is larger when the self and cross couplings a and b are similar in magnitude, whereas for higher noise correlations \mathcal{M} -information is maximised for asymmetric interactions (Fig. 6).

3. Further analyses on mouse brain

Here we complement the Neuropixel results presented in the main article with additional insights. First, we look at the behaviour of Mutual information, \mathcal{W} -information, and (non-normalised) \mathcal{M} -information (Fig. 7).

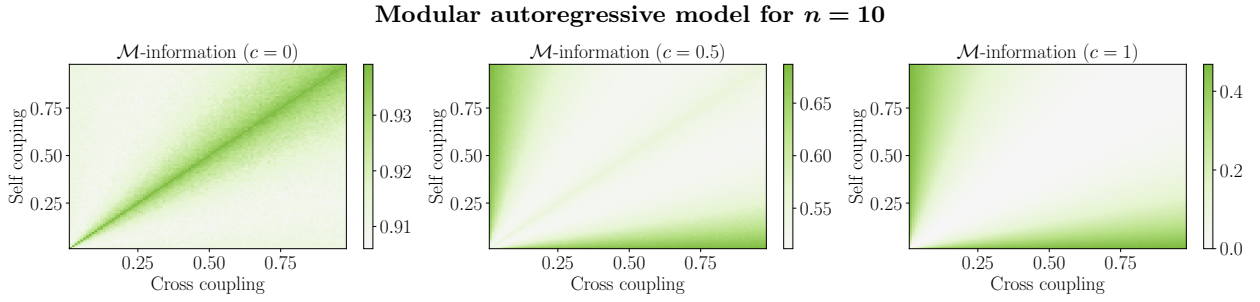


FIG. 6: Modular VAR model for $n = 10$ time series, with parameters given by Eq. (E1). For low values of noise, \mathcal{M} -information is larger for comparable self and cross coupling. For higher noise correlations, \mathcal{M} -information is maximised when either the self coupling is high and the cross coupling is low, or vice versa.

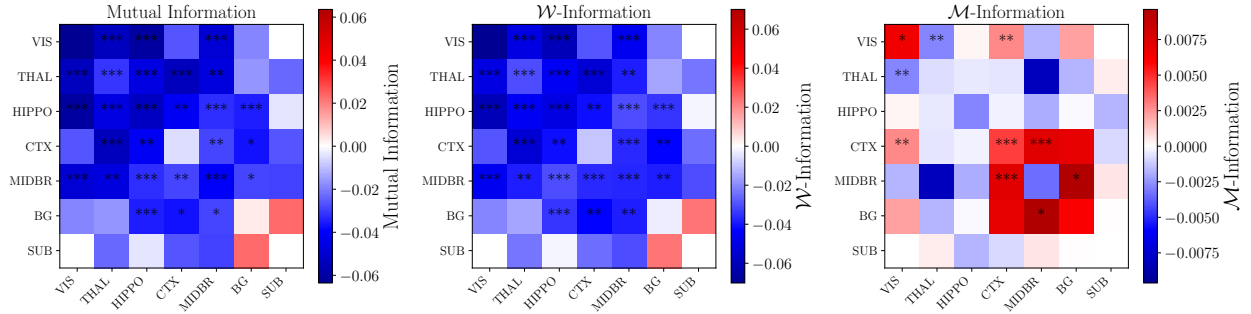


FIG. 7: Mutual information, \mathcal{W} -information, and \mathcal{M} -information per brain region for correct-incorrect trials. (P-values calculated with a one-sample t-test against the zero-mean null hypothesis. *: $p < 0.05$; **: $p < 0.01$; ***: $p < 0.001$).

We notice that the mutual information is significantly higher in the incorrect condition, which can be attributed to a decrease in entropy rate of the neural signal⁴. We observe consistently lower \mathcal{W} -information for correct trials, and topographically-specific increases and decreases in \mathcal{M} -information. However, to make more robust comparisons across different systems, a normalisation procedure is needed to factor out the contribution of the mutual information magnitude [55]. Hence, in the main body of the work we showed the values of \mathcal{M} -information normalised by the joint mutual information. To complement those results, here we also report the behaviour of normalised \mathcal{W} -information, which unexpectedly shows the opposite trend than normalised \mathcal{M} -information (Fig. 8).

Finally, we focus on the \mathcal{M} -information calculated between specific theory-driven regions of interest in the mouse brain (Fig. 9). Namely, we consider:

- **VISp** – Primary Visual Cortex
- **CL** – Central Lateral Nucleus
- **LGd** – dorsal Lateral Geniculate Nucleus
- **LP** – Lateral Posterior Nucleus
- **MD** – Mediodorsal Nucleus
- **POL** – Posterior Lateral Visual Area
- **CA1** – Cornu Ammonis Area 1
- **ACA** – Anterior Cingulate Area

⁴ The sum of entropy rate and mutual information should yield the total entropy of the time series, which we normalised to 1. Hence, an increase in entropy rate is equivalent to a decrease in mutual information, and vice versa.

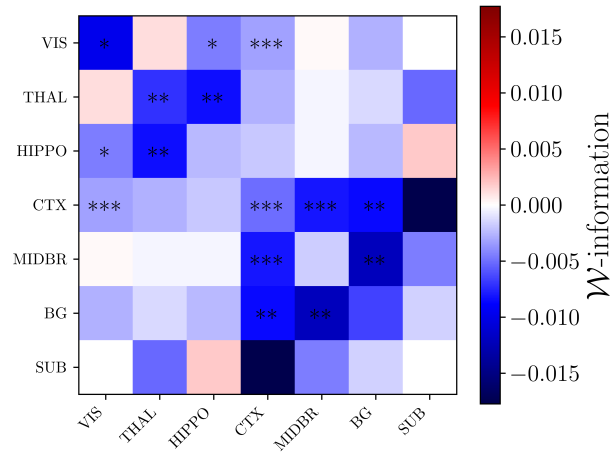


FIG. 8: Normalised \mathcal{W} -information per brain region for correct-incorrect trials. (P-values calculated with a one-sample t-test against the zero-mean null hypothesis. *: $p < 0.05$; **: $p < 0.01$; ***: $p < 0.001$).

- **ILA** – Infralimbic Area
- **RSP** – Retrosplenial Area

As expected, we observe an increase in \mathcal{M} -information between early visual cortex and every other key cortical and subcortical region. Thus, despite our previous observations showing no increase in high-order thalamo-visual interactions during correct perceptual performance, we find an increase in specific instrumental thalamic nuclei such as the LGd, LP and MD. This provides preliminary evidence that low-level sensory subsystems may support perceptually relevant high-order information structures. Hence, the thalamus, far from being a simple relay station, might possess the capacity for complex macroscopic computation.

We emphasise that these findings are only suggestive of the behaviours discussed, as the small sample size prevented statistical validation. A promising avenue for future work is to rigorously test the hypotheses presented above.

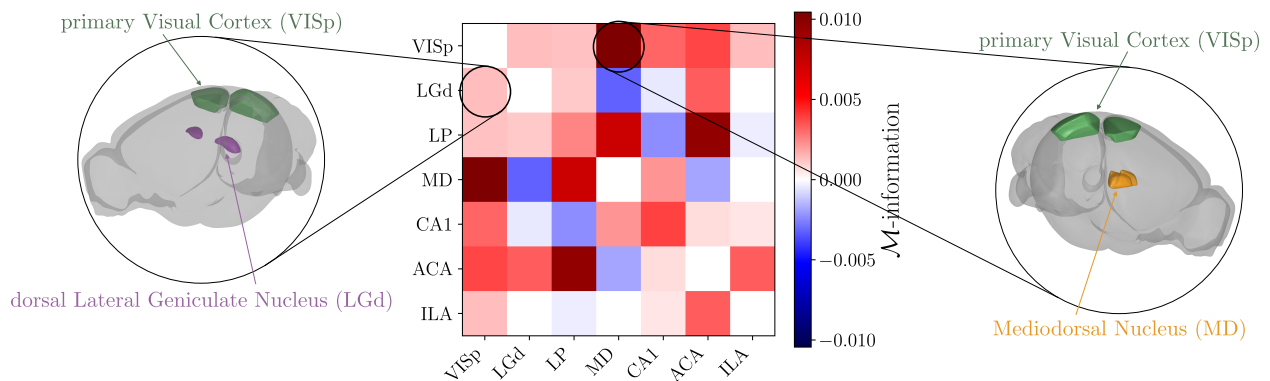


FIG. 9: Normalised \mathcal{M} -information on correct-incorrect trials for specific regions of interest in the mouse brain.